

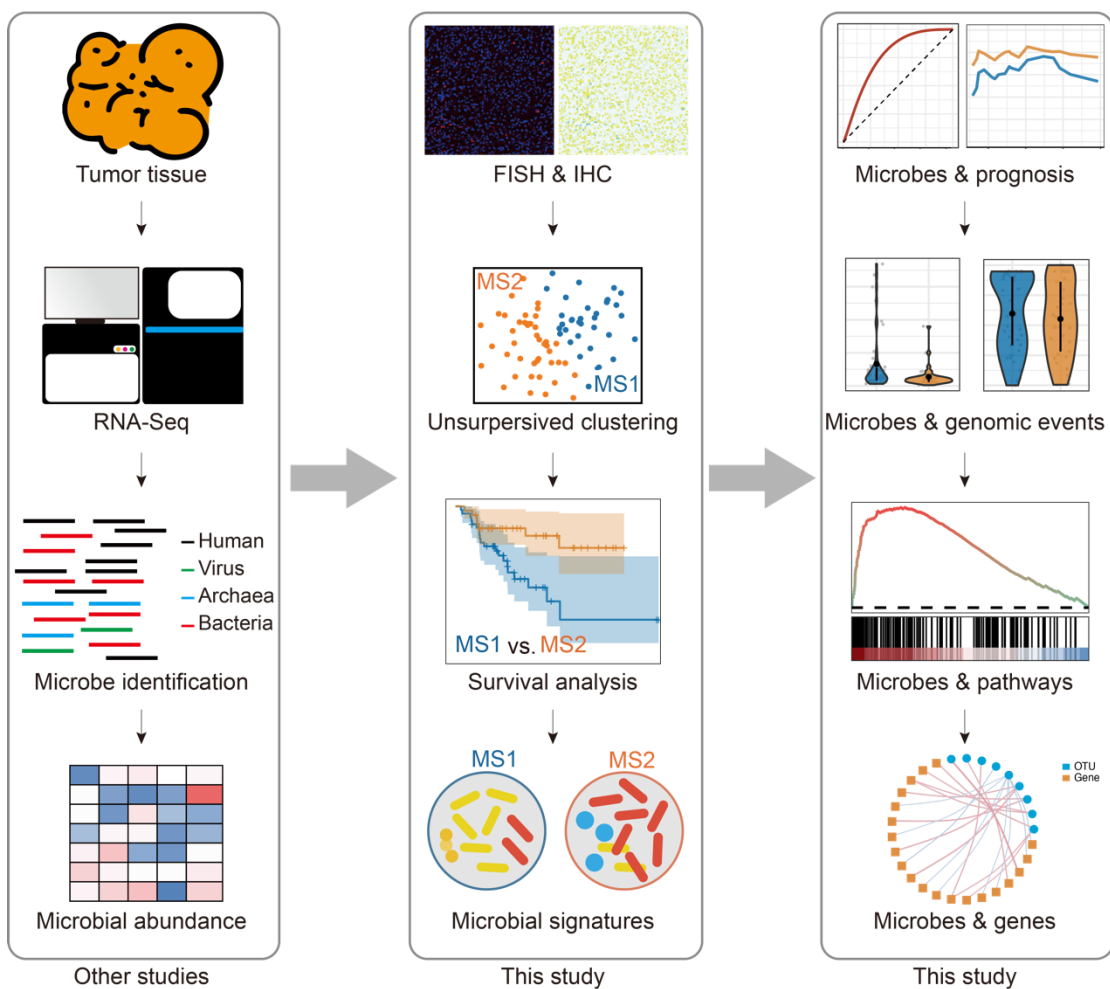
Supplementary Materials

Contents

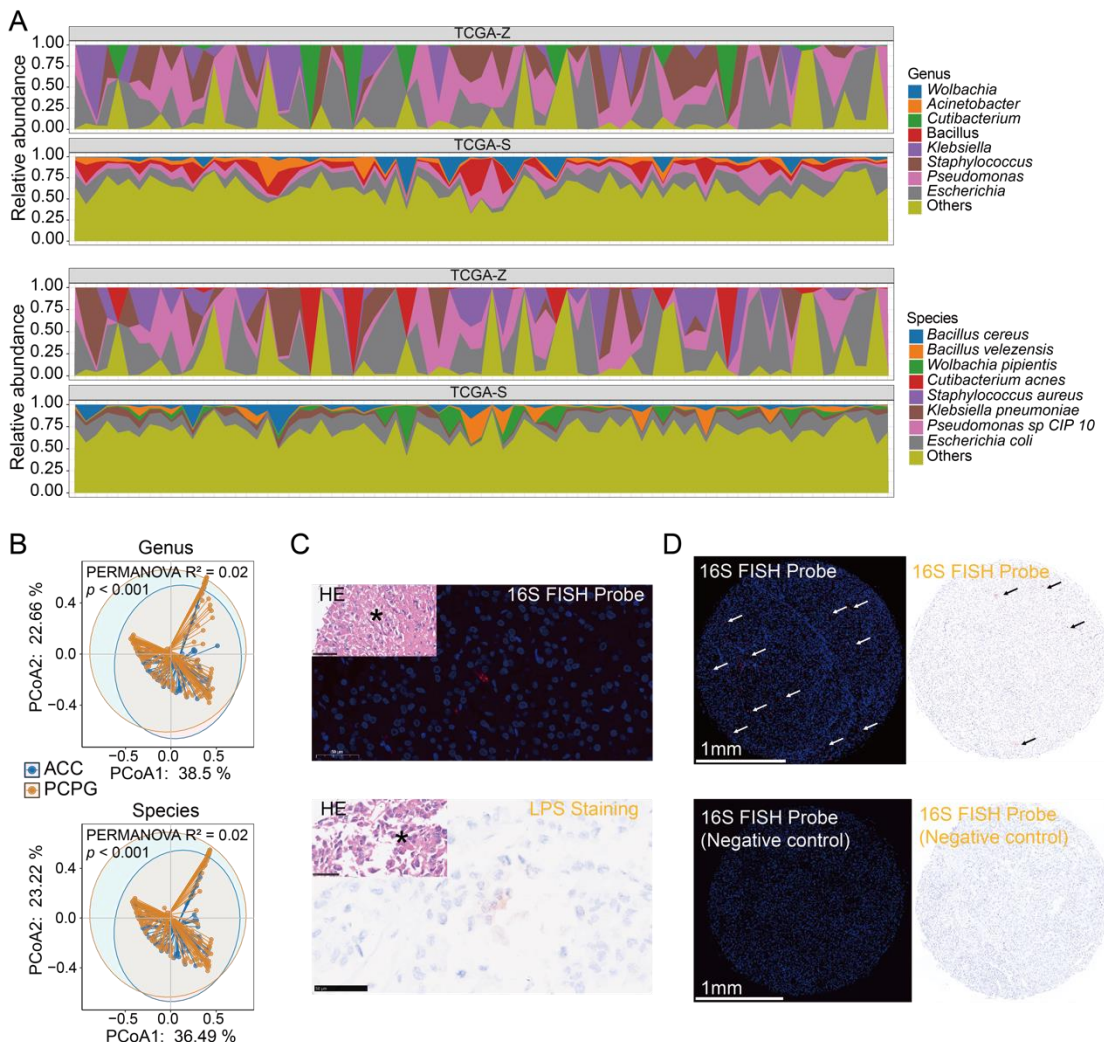
Part I Re-analyzed Figures	3
(R) <i>Figure 1. Overview of the analysis pipeline.</i>	3
(R) <i>Figure 2. ACC harbors intratumor microbes.</i>	4
(R) <i>Figure 3. Intratumoral microbial composition is associated with prognosis in TCGA-S dataset.</i>	5
(R) <i>Figure 4. Intratumoral microbial signatures improve prognosis prediction in TCGA-S dataset.</i>	6
(R) <i>Figure 5. Intratumoral microbial composition is associated with host genomic events.</i>	7
(R) <i>Figure 6. Microbial subgroup is associated with immunity.</i>	8
(R) <i>Figure 7. Intratumoral microbiota might activate carcinogenic pathways.</i>	9
 Part II Re-analyzed Main Text.....	 10
Title.....	10
Abstract.....	10
Keywords.....	10
Highlights.....	10
INTRODUCTION.....	11
RESULTS.....	12
ACC Harbors Intratumoral Microbes	12
Intratumoral Microbiome Composition Is Associated with Prognosis in ACC	13
Intratumoral Microbial Signatures Can Improve Prognosis Prediction	14
Intratumoral Microbial Composition is Associated with Host Genomic Events	15
Intratumoral Microbial Composition is Associated with Immunity	16
Intratumoral Microbiota Might Activate Carcinogenic Pathways	17
DISCUSSION.....	17
CONCLUSION.....	22
METHODS.....	22
Data Acquisition	22
Preprocessing microbiome data	23
Unsupervised Clustering for Microbiome Data	23
Alpha Diversity and Beta Diversity of Microbial Communities	24
Identification of Microbes with Different Abundance	24
Microbial Risk Score Model Construction	24
Kaplan–Meier Curves	25

Prognostic Prediction Measurement	25
Somatic Variant Analysis	26
Tumor Immune and Metabolism Estimation	26
Differentially Expressed Gene Analysis and Gene Set Enrichment Analysis	26
Microbe-Host Gene Interaction	26
16S rRNA Staining (Direct-Labeling RNA In Situ Hybridization)	27
Immunohistochemistry (IHC) of LPS	27
Statistical Analysis	27
References	28
Part III Re-analyzed Supplementary Figures	37
<i>(R) Figure S1. The number of microbes detected in two datasets.</i>	37
<i>(R) Figure S2. Intratumoral microbial composition is associated with prognosis in TCGA-Z dataset.</i>	38
<i>(R) Figure S3. Association between clusters and overall survival and progression-free survival.</i>	39
<i>(R) Figure S4. Intratumoral microbial signatures improve prognosis prediction in TCGA-Z dataset.</i>	40
<i>(R) Figure S5. Survival distribution based on the abundance levels of 7 microbial signatures in TCGA-S dataset.</i>	42
<i>(R) Figure S6. Survival distribution based on the abundance levels of 7 microbial signatures in TCGA-Z dataset.</i>	43
<i>(R) Figure S7. Landscape of copy number variations and driver mutations within two microbial subgroups.</i>	44
<i>(R) Figure S8. Pathway enrichment of the genomic events within two microbial subgroups.</i>	45
<i>(R) Figure S9. Microbial subgroup is associated with immune cell infiltrations.</i>	46
<i>(R) Figure S10. Gene set enrichment analysis between microbial subgroups.</i>	47
<i>(R) Figure S11. The correlation between microbial subgroup and molecular phenotypes.</i>	48
<i>(R) Figure S12. Microbial subgroup is associated with metabolism.</i>	49
<i>(R) Figure S13. Links between microbial taxa and host genes in pathways.</i>	50
Part IV Re-analyzed Supplementary Tables	51
<i>(R) Table S1. Chi-squared test of various clinical parameters between two subgroups.</i>	51
<i>(R) Table S2. PERMANOVA test on clinical factors.</i>	52
<i>(R) Table S3. Chi-squared test of various genomic events between two subgroups.</i>	53

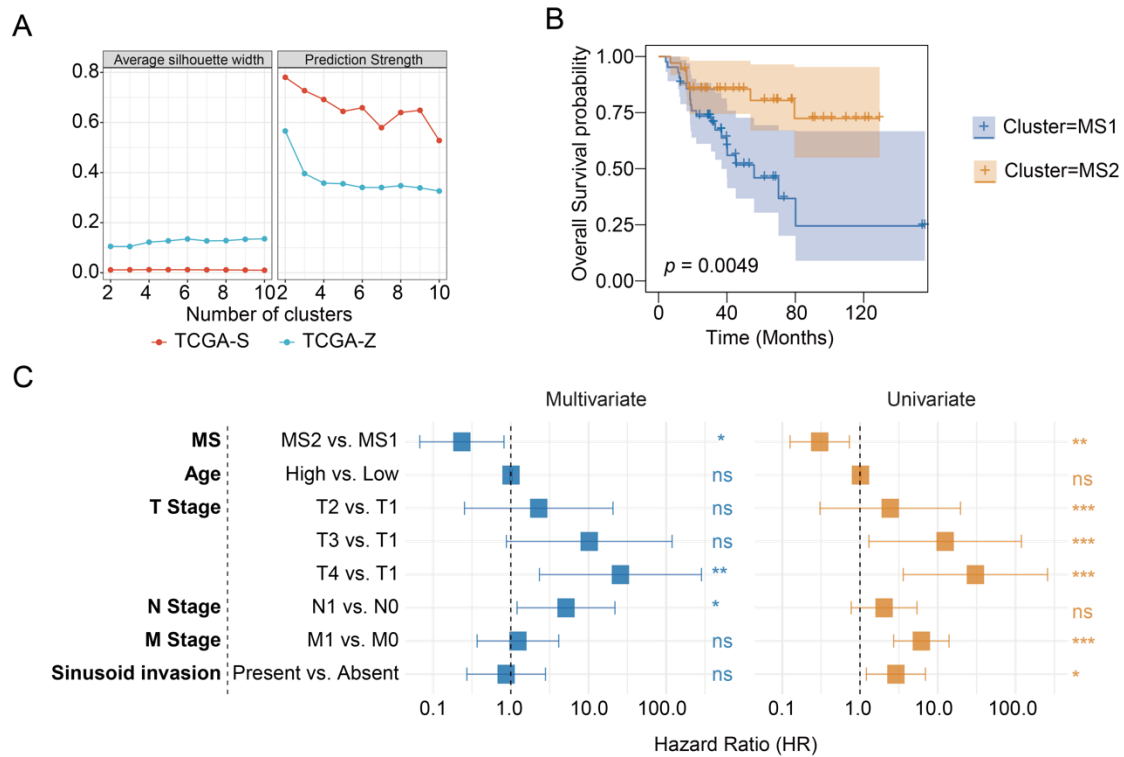
Part I Re-analyzed Figures



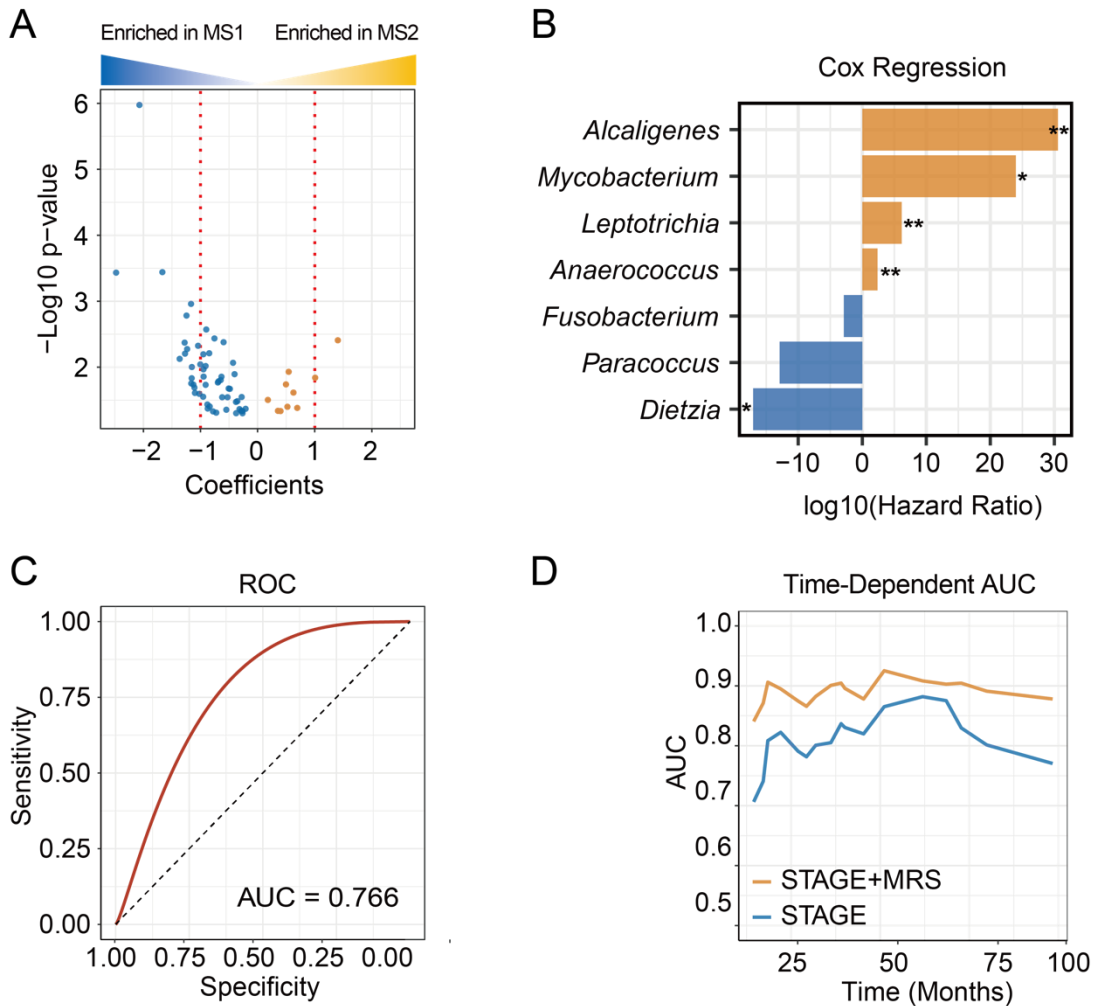
(R) Figure 1. Overview of the analysis pipeline. TCGA primary tumors were subject to RNA-Seq, in which microbial abundance (comprising virus, archaea, and bacteria) was identified and normalized in other studies (left panel). To confirm the presence of intratumor bacteria, 37 ACC tissue microarray chips from the in-house cohort were stained for FISH and IHC examination. Unsupervised clustering was performed on microbiome data to explore natural clusters of patients with distinct microbiomes, thereby influencing prognoses. The microbial signatures associated with prognosis were further determined (middle panel). Defined microbial signatures were tested to improve prognosis prediction. The intratumoral microbiome was found to be associated with biological pathways involving cell cycle, tumor immunity, and metabolism (right panel).



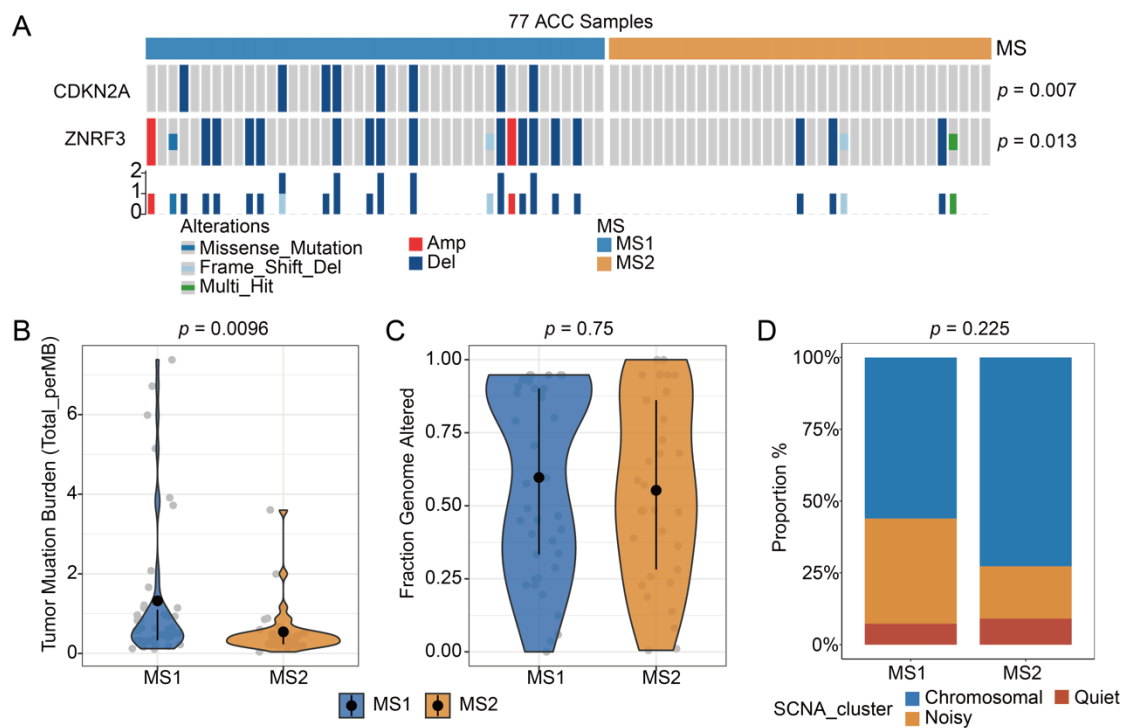
(R) Figure 2. ACC harbors intratumor microbes. (A) Relative abundance of microbes in two datasets at genus and species levels. Only the top five taxa of each microbiome data were shown. (B) Principal coordinate analysis (PCoA) for ACC and PCPG, based on the Bray-Curtis dissimilarity. Permutational multivariate analysis of variance (PERMANOVA) gave the p value. (C) Representative images of FISH staining of 16S rRNA (upper panel) and IHC staining of LPS (lower panel) in tissue sections from 37 ACC samples. (D) Representative images of comparison between positive signals (upper panel) and the negative controls (lower panel) in FISH staining of 16S rRNA (left) and IHC staining of LPS (right). Arrows indicate positive staining signals.



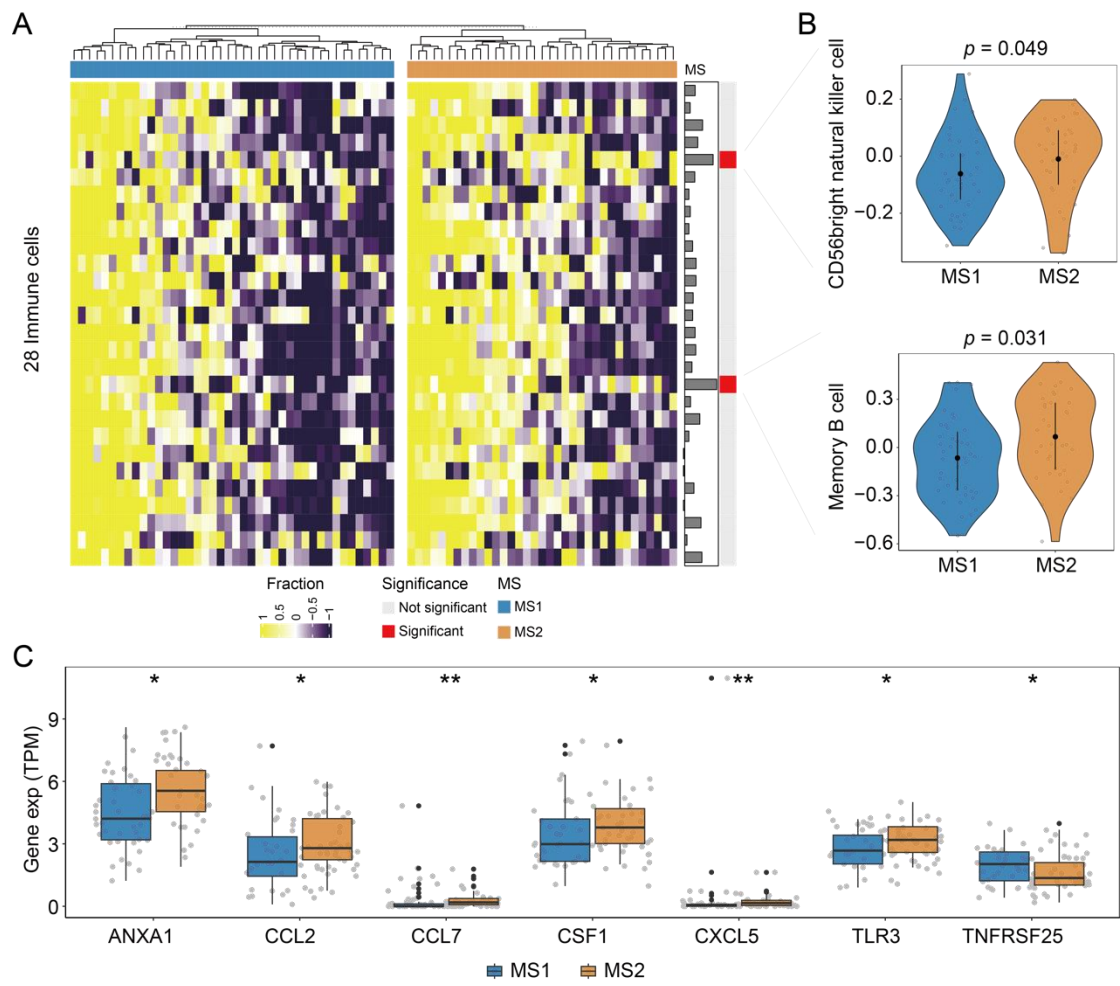
(R) Figure 3. Intratumoral microbial composition is associated with prognosis in TCGA-S dataset. (A) Clustering scores of different cluster numbers. The quality of clustering was estimated by silhouette width and prediction strength. (B) Kaplan-Meier plot of two subgroups in TCGA-S clustering. The Log-rank test gave the p value. (C) Multivariate and univariate cox analysis of microbial subgrouping, and other clinical factors usually considered impacting overall survival. The significance was shown with asterisks.
 $*p < 0.05$; $**p < 0.01$; $***p < 0.001$; ns, Not Significant.



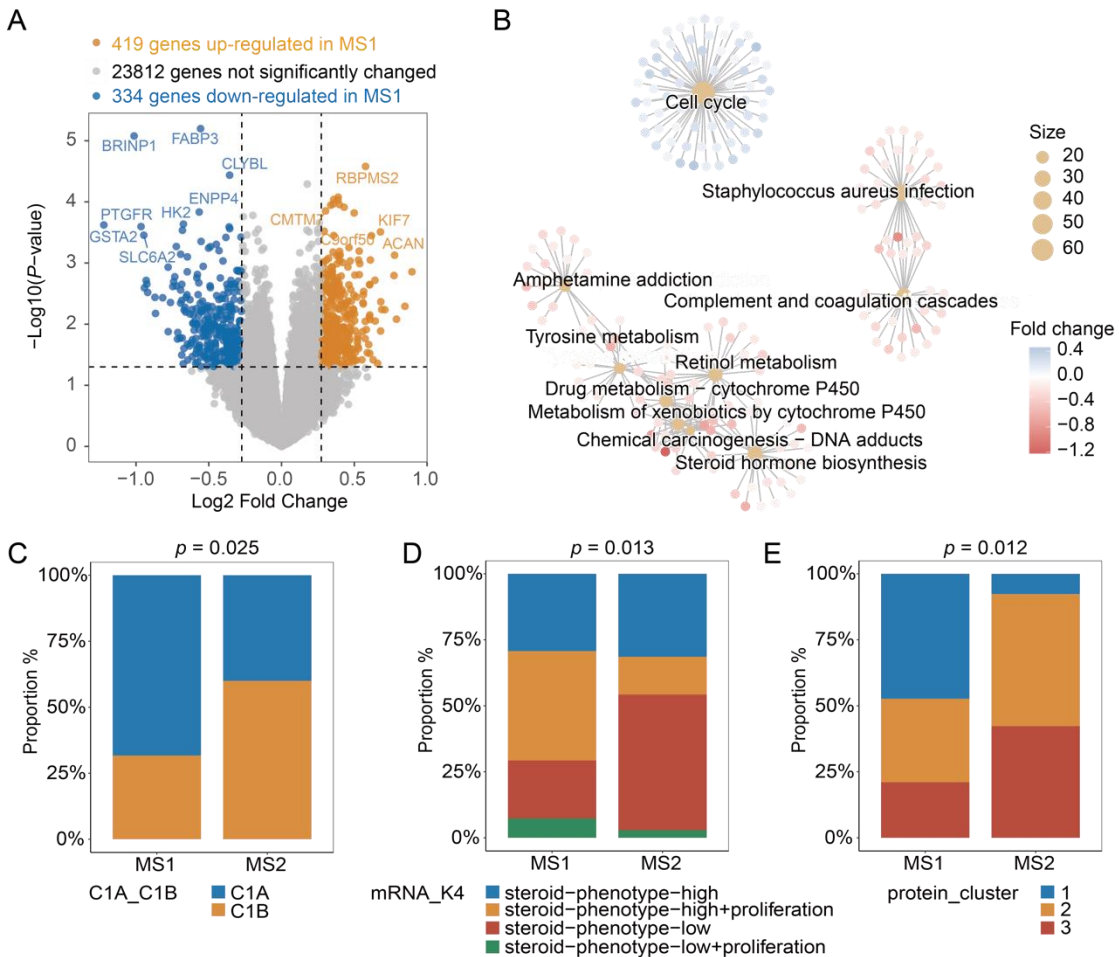
(R) Figure 4. Intratumoral microbial signatures improve prognosis prediction in TCGA-S dataset. (A) Volcano plot showing different genera resulting from MaAsLin2. Y-axis is the -Log₁₀ (p values), and X-axis is the coefficients. Each dot denotes one genus. (B) Bar plot showed the hazard ratio of each genus in cox regression analysis. A hazard ratio of > 1 (\log_{10} HR > 0) means a high abundance of the genus damages prognosis, while that <1 (\log_{10} HR < 0) means a high abundance of the genus benefits prognosis. (C) Receiver operation curves of 7 genera-based microbial risk score (MRS) as predictive of overall status in TCGA-S dataset. The area under curves suggests the predicting capability of overall survival. (D) Area under curve (AUC) for overall survival between clinical stage alone and stage plus MRS in a time-dependent manner in TCGA-S dataset. * $p < 0.05$; ** $p < 0.01$.



(R) Figure 5. Intratumoral microbial composition is associated with host genomic events. (A) Waterfall plot showing the differentially distributed genomic events in ACC categorized by MS in TCGA-S clustering. Chi-squared or Fisher's exact test gave the p value. Violin plot showing the difference of (B) tumor mutation burden (TMB) and (C) fraction genome altered (FGA) between microbial subgroups in TCGA-S clustering. (D) Stacked bar plot showing chi-squared test of somatic copy number alteration (SCNA) cluster between MS1 and MS2.



(R) Figure 6. Microbial subgroup is associated with immunity. (A) Heatmap showing the proportions of 28 immune cells in tumor microenvironment between two microbial subgroups in TCGA-S clustering. Wilcoxon rank test gave the p value. (B) Violin plot showing the difference of CD56bright natural killer cell and memory B cell percentage within tumors between microbial subgroups. (C) Box plot showing the difference of immune-related gene expression between microbial subgroups. The significance was shown with asterisks. $*p < 0.05$; $**p < 0.01$.



(R) Figure 7. Intratumoral microbiota might activate carcinogenic pathways. (A) Volcano plot showing the differentially expressed genes between MS1 and MS2. The X axis refer to log transformed fold change, and the Y axis represent the $-\text{Log}_{10}(p \text{ value})$. (B) Net plot showing the top 10 pathways significantly enriched based on the differential genes. The size of the dot represents the gene counts contributing to the pathway. Stacked bar plot showing chi-squared test of (C) C1A/C1B cluster, (D) mRNA cluster, (E) methylation cluster proportions between MS1 and MS2 in TCGA-S clustering.

Part II Re-analyzed Main Text

(Note: The modifications are highlighted in red)

Title

Intratumoral microbiota is associated with prognosis in patients with adrenocortical carcinoma

Abstract

Adrenocortical carcinoma (ACC) is a rare but aggressive malignancy. Recent studies have discovered a pivotal role of the intratumoral microbiota in various cancers, yet it remains elusive in ACC. Here, we explored the intratumoral microbiome data derived from in silico identification, further validated in an in-house cohort by bacterial 16S rRNA fluorescence in situ hybridization and lipopolysaccharide staining. Unsupervised clustering determined two naturally distinct clusters of the intratumoral microbiome in ACC, which was associated with overall survival. The incorporation of microbial signatures enhanced the prognostic performance of the clinical stage. Genetic and transcriptomic association analyses further demonstrated that microbiome-defined subgroups exhibited differential activation of cell cycle pathways, along with distinct immune and metabolic profiles. Our study not only supports the presence of intratumoral bacteria but also implies a prognostic and biological role of intratumoral microbiota in ACC, which can advance a better understanding of the biology of ACC.

Keywords

adrenocortical carcinoma, intratumoral microbiota, microbiome, prognosis

Highlights

- Adrenocortical carcinoma harbors intratumoral microbes.
- The intratumoral microbiome is associated with prognosis in ACC.
- The intratumoral microbiota might correlate with genomic events, immune status, and specific carcinogenic pathways.

INTRODUCTION

Adrenocortical carcinoma (ACC) is a rare but aggressive disease. Although hormone excess is present in ~50% of cases, most patients are diagnosed at an advanced stage, which confers a 5-year survival of less than 10% [36]. As an orphan disease, the only phase III clinical trial (namely, FIRM-ACT trial) of advanced ACC recommending an EDP+M regimen (etoposide, doxorubicin, cisplatin, and mitotane) showed a moderate effect on survival improvement [37]. A profound understanding of the biology of ACC may contribute substantially to novel treatment modalities.

Next-generation sequencing (NGS) has enabled us to gain deeper insight into genetic and genomic alterations in ACC. To date, with NGS technologies, The Cancer Genome Atlas (TCGA) and genomic profiling by Assié et al. have depicted an unprecedented genomic understanding of this rare disease [10]. Genetic driver events include mutations in TP53, CTNNB1, MEN1, PRKAR1A, RPL22, NF1, and MLL4, as well as whole-genome doubling (WGD), together with several mRNA and methylation signatures that are prognostic [8]. In addition to providing a landscape of host genetics, NGS data from tissue or blood were found to smuggle the genetic materials of microorganisms, providing an opportunity to gain a deeper understanding of the intratumoral microbiome [1,38].

Cancer-resident microorganisms, especially intratumoral bacteria (ITB), have recently been revealed to play a critical role in several cancer types [38–40]. Studies on cancer-associated microbiology have gone through three eras in general. Conventional pathology-based studies solely identified limited carcinogenic microbiomes, such as *Helicobacter pylori* in gastric cancer and hepatitis B virus in liver cancer [41,42]. Although limited in number, many such studies drastically updated the understanding and treatment of the disease. In the second era, which is still extending today, cancers originating from “contaminated” organs, or the gastrointestinal tract were targeted [43]. The gut microbiome is now considered omnipotent in mediating various physio- and pathophysiological activities, including cancer [43–48]. Metabolites of gut bacteria not only promote local carcinogenesis but also mediate the drug sensitivity of targeted or immunotherapy of other

organs [43]. Only recently have scholars been able to develop algorithms to characterize intratumoral microbes from NGS data focusing on investigating host physiology rather than resident microbes and, thus, revolutionizing our understanding of intratumoral microbiome in various cancers [39,40]. Interrogation of the functional role of intratumoral microbiome is of great interest, propelling onco-microbiology into the third era.

Despite being associated with various tumors, the intratumoral microbiota remains uncharacterized in ACC. To bridge this gap, this study, for the first time, delineates the characteristics of the intratumoral microbiota in ACC. By exploiting the intratumoral microbiome data characterized by Sheng et al. [1] and Salzberg et al. [2,3], we found that the intratumoral microbiome is associated with prognosis, host genomic events, and carcinogenic pathway activation in ACC. Additionally, microbial signatures could improve prognosis prediction compared with stage alone. Our study holds promise for a better understanding of the biology and for developing novel treatment strategies in ACC.

RESULTS

ACC Harbors Intratumoral Microbes

To illuminate the intratumoral microbiota in ACC, we revisited and obtained the intratumoral microbial profiles in different cancers, as previously processed by two independent studies: the TCGA-Z dataset (Sheng et al. [1]) and TCGA-S dataset [2,3] (data shared by Salzberg) ((R) Figure 1). The intratumoral microbes comprised three types of microorganisms (i.e., viruses, archaea, and bacteria). Normalization and decontamination were also included according to different criteria. The ACC samples in TCGA consist of 79 RNA-Seq data from the primary tumor of 79 patients, in which poly(A) enrichment of the mRNA was used when preparing RNA-Seq libraries. For microbial profiling, notably, both Sheng et al. and Salzberg et al. analyzed the raw BAM files from RNA sequencing to identify and extract microbial reads in ACC samples.

We next examined the microbial profile in ACC within two datasets. A total of 1854 and 1669 genera, and 6916 and 5619 species were included in the TCGA-Z and TCGA-S datasets, respectively ((R) Figure S1). The genera *Escherichia* and *Pseudomonas* were

the most abundant in two datasets, while the species *Escherichia coli* was consistently the most predominant in the above data ((R) **Figure 2A**). As TCGA-ACC cohort lacked paired normal control, we opted for adrenal pheochromocytoma (PCPG) as the control to exclude tumor context, in view of their similar site and surgical procedure. Principal coordinate analysis (PCoA) showed a significantly distinct microbiome composition between PCPG ($n = 178$) and ACC ($n = 79$) (permutational multivariate analysis of variance (PERMANOVA) test, $P < 0.001$), implying that the intratumoral microbiome was tumor type-dependent ((R) **Figure 2B**).

To confirm the presence of microbes in ACC, especially the most abundant bacteria, we stained the ACC tissue microarray chip (TMA) containing 37 samples from our in-house cohort. With a universal probe against bacterial 16S rRNA, we adopted RNA fluorescence in situ hybridization (FISH) for detecting bacterial RNA in ACC tissue ((R) **Figure 2C**). We also performed immunohistochemistry (IHC) staining against bacterial lipopolysaccharide (LPS), which is specific to detecting Gram-negative bacteria ((R) **Figure 2C**). Positive 16S rRNA and LPS staining was identified in 97.3% (36/37) and 83.8% (31/37) of ACC samples, respectively, indicating the actual presence of bacteria in ACC ((R) **Figure 2D**).

Intratumoral Microbiome Composition Is Associated with Prognosis in ACC

Considering the possible relationship between tumor microbiome and cancer prognosis [49], we sought to determine whether intratumoral microbiome composition could influence prognosis in ACC. We speculated that naturally distinct clusters of the intratumoral microbiome might be associated with ACC prognosis. For this purpose, an unsupervised clustering strategy, partition around medoids (PAM) clustering [11], was applied to microbial abundance data (genus level) of 77 patients from both TCGA-Z and TCGA-S datasets (excluding two patients missing cancer stage). Prediction strength (PS) and silhouette index (SI) were used to assess the cluster number and quality of the according clusters. We observed a low PS (<0.8) and SI (<0.5), signifying weak support for clustering ((R) **Figure 3A**), probably due to limited data size, potential contaminants, or no substantial difference in ACC intratumoral microbiome. This unsupervised clustering based on

microbial composition, thus, grouped patients into two clusters. In the remainder of the paper, the two clusters of patients are termed MS1 (microbial subgroup 1) and MS2 cohorts.

We then used principal coordinate analysis (PCoA), based on BC dissimilarity, to confirm the difference in the microbial community between each pair of MS1 and MS2. As expected, we found a significant difference (PERMANOVA test, $P < 0.05$) between two MS cohorts in both microbial abundance datasets (**((R) Figure S2A-B)**). The alpha diversity of the MS cohorts was also assessed using the Shannon index. MS1 displayed a significantly different diversity (Wilcoxon signed-rank test, $P < 0.05$) with MS2 (**((R) Figure S2A-B)**).

We then attempted to interrogate the prognostic difference between the two MS cohorts. To do this, we adopted the Kaplan–Meier estimate for examining the survival distribution [50], using the log-rank test to test the difference between two subgroups. A significantly higher overall survival probability in MS2 than MS1 was observed when applying TCGA-S clustering ($P < 0.01$, **((R) Figure 3B)**). In contrast, neither overall survival nor progression-free survival difference was found using TCGA-Z clustering (**((R) Figure S3A-B)**). These results suggest an association between intratumoral microbiome composition and prognosis in ACC.

Lastly, we assessed the clinical characteristics between the two MS cohorts. We found that the MS1 cohort (worsened prognosis) was enriched with **sinusoid invasion (Present: 57.14% vs. Absent: 16.67%, Fisher's exact test, $P < 0.05$)** (**((R) Table S1)**). To determine whether the microbial composition could function as an independent prognostic biomarker, Cox analysis was performed, which showed that microbiota subtype, as well as **T4 stage and N1 stage, succeed** to predict prognosis independently in ACC cohorts (**((R) Figure 3C)**).

Intratumoral Microbial Signatures Can Improve Prognosis Prediction

Given that microbes can alter prognosis [51], we asked whether any microbe impinge on prognosis in ACC. As several clinical factors (e.g., age, gender, race, and clinical stage) might be associated with microbiome composition [52], we first sought to examine potential confounders of microbial signatures. The confounding effects of 12 clinical factors were quantified by the PERMANOVA test according to the Bray-Curtis dissimilarity (**((R) Table**

S2). We observed that no other clinical factors influenced the microbiome composition.

We then used MaAsLin2 [18] and ANCOM [19] to determine the significantly different genera between two MS cohorts (**(R) Figure S4A**). When applying TCGA-S clustering to TCGA-S data, 17 genera were found to be significantly different between two MS cohorts (FDR < 0.05), of which 16 were commonly identified across both datasets (**(R) Figure 4A**). To further determine the microbial signatures that might be associated with prognosis, we performed the Cox proportional hazards regression model. A total of 7 genera was identified to construct the microbial risk score (MRS) based on their coefficient and abundance (**(R) Figure 4B**). The dead patients possess a higher microbial risk score than those alive in both datasets (**(R) Figure S4B-C**). We next stratified patients into two groups individually according to the median abundance of 7 genus features. The difference in survival distribution was confirmed by the Kaplan–Meier estimate (**(R) Figure S5, S6**), reinforcing that the high abundance of the 2 genera, including *Anaerococcus* and *Leptotrichia*, were closely associated with an unfavorable prognosis.

There are a limited number of reports on ACC prognostic biomarkers. Previous studies tried to construct a microarray-based prognostic predictor and identified several genes as optimal predictors [53,54]. To evaluate the predictive ability of OS using MRS, we performed area under curve (AUC) receiver operator characteristic (ROC) analysis. Surprisingly, the MRS in our study showed an AUC of 0.766 in TCGA-S dataset (**(R) Figure 4C**), and 0.773 in TCGA-Z microbiome data in predicting OS (**(R) Figure S4D**). Furthermore, we found that incorporation of MRS enhanced performance of stage alone on prognosis prediction (**(R) Figure 4D, (R) Figure S4E-G**). This corresponds to another model that tumor microbial abundances, alone or in combination with tumor gene expression, can predict cancer prognosis and drug response to some extent [49].

Intratumoral Microbial Composition is Associated with Host Genomic Events

A large-scale study identified several significantly mutated genes in ACC and showed recurrent somatic copy number variations (CNVs) [4]. Therefore, we next attempted to depict the landscape of genetic mutation and CNVs of these patients. We compared the

occurrence of various genomic events between two MS cohorts using the chi-squared test and observed a higher rate of **CDKN2A** (cytoband: 9p 21.3) loss and **ZNRF3** (cytoband: 22q 12.1) loss in MS1 ((R) **Table S3**, (R) **Figure 5A**, (R) **Figure S7**). We then compared the genomic events between two subgroups by fraction of samples affected, and found that those belonging to cell cycle pathway, **WNT pathway**, and **Hippo signaling pathway** were significantly different ((R) **Figure S8**), which are the commonly activated pathway in most ACC tumors.

We also compared tumor mutation burden (TMB) between two cohorts and found a higher TMB in the MS1 cohort, consistent with the previous finding that a high TMB level is associated with a worse prognosis [55] ((R) **Figure 5B**). Although no difference in fraction genome alteration (FGA) was observed, MS1 was significantly enriched with a noisy somatic copy number alteration (SCNA) cluster, which is characterized as an aggressive disease phenotype [8] ((R) **Figure 5C-D**).

Intratumoral Microbial Composition is Associated with Immunity

ACC is characterized by indolent immunity and immunotherapy resistance [56]. To evaluate the immune status within two MS cohorts, we estimated 28 immune cell types infiltrating and employed other four complementary computational methods, where we observed a lower proportion of tumor-infiltrating lymphocytes (TILs) in the MS1 cohort ((R) **Figure 6A**, (R) **Figure S9**), including inactivated memory B cell, and CD56bright natural killer T cell ((R) **Figure 6B**). A difference in these immune cells was also observed in other solid tumors such as breast and lung cancers [57,58]. As many of intratumoral microbiota effects on the TME appear to suppress local antitumor immunity [59], we next interrogated the immune regulatory genes related to multiple immune cells. Accordingly, we identified several genes, including macrophage positively related genes (**CSF1**, **CCL2**) and other immune-stimulating genes (such as **ANXA1**, **TLR3**, **TNFRSF25**, and **CXCL5**), were downregulated in the MS1 cohort ((R) **Figure 6C**).

Intratumoral Microbiota Might Activate Carcinogenic Pathways

An insightful understanding of microorganism-associated molecular pathways (MAMPs) is a standard procedure to identify the “friend or foe” role of the intratumoral microbiota. We first explored host transcriptomics in ACC to determine differentially expressed genes (DEGs) between two MS cohorts. KEGG pathway enrichment analysis of DEGs ((R) **Figure 7A**) revealed the top 10 enriched pathways when applying TCGA-S clusters ((R) **Figure 7B**). Considering the signaling pathways related to ACC progression and those related to microbiota reported elsewhere, the cell cycle and some immune- and metabolism- related pathways attracted our attention. The differential activities of these pathways between subgroups were also validated using gene set enrichment analysis ((R) **Figure S10**).

Then we performed systematic comparison between microbial subgroups and established molecular subtypes proposed by Zheng et al. [8]. The MS1 cohort was enriched with an aggressive transcriptomic subtype of C1A and steroid phenotype high [8] ((R) **Figure 7C-D**). The transcriptomic subtype of C1A and steroid phenotype high was defined as malignant tumors showing a worse prognosis according to gene expression analysis in a study, which could be used as an independent prognostic biomarker in addition to pathology and tumor staging; this has been accepted as a robust predictor [60]. Additionally, MS1 showed a higher proportion of protein cluster 1 ((R) **Figure 7E**), indicating a more malignant phenotype in MS1. However, we did not observe any association between the MS signature and signatures of histology, DNA methylation level, or miRNA ((R) **Figure S11**).

DISCUSSION

In this study, we took advantage of microbial abundance generated by Sheng et al. and Salzberg et al. to undertake a systematic investigation of the intratumoral microbiome in ACC. Using bacterial 16S rRNA FISH and LPS staining, we also validated the presence of ITB in our in-house cohort. The unsupervised clustering method inferred two naturally distinct clusters of intratumoral microbiome in ACC, which were associated with overall survival. Incorporating microbial risk score could improve the predictive ability of disease

status compared with that only based on the clinical staging. Additionally, the intratumoral microbiome was also found to be associated with host genomic events and carcinogenic pathways. In summary, our study provides deep insight into the intratumoral microbiome for ACC, and it could stimulate future studies on how the intratumoral microbiome could guide targeted therapies and immunotherapies.

The intratumoral microbiota has been discovered in most, if not all, human cancers, including in adjacent normal and deep tumor tissues, which are usually considered sterile. However, the composition of intratumoral microbiota varies drastically per different cancer types [39,61]. Consistent with previous studies of different solid tumors, we, for the first time, observed the presence of ITB in over 80–90% samples of ACC using 16S rRNA FISH and LPS staining. Whether residing within or close to the tumor and/or TILs, the intratumoral microbiota shows strong cancer type-dependent characteristics [39,61]. Indeed, we found a significant difference in intratumoral microbiome between ACC and PCPG, although they are remarkably similar concerning the site and surgical procedure. Therefore, the intratumoral microbiome uniqueness might serve as a biomarker for identification or diagnosis, as claimed by some scientists [39]. Additionally, emerging studies highlighted the intra-tumoral microbial influence on more clinical phenotypes such as tumor relapse [62], tumor metastasis [40], and prognosis [51] of patients. Recently, the mechanism of the tumor-resident microbiota affecting the tumor biology has become a study hotspot. For example, tumor-resident *F. nucleatum* triggers the GalNAc/autophagy/TBC1D5 signaling in oral squamous cell carcinoma (OSCC), driving tumor-associated macrophage (TAM) formation and OSCC progression [63]. Following this trend, our study proposes the prognostic role of the intratumoral microbiome, with the aim of comprehensively characterizing the potential biological roles, which can pave the way for a deeper study.

Unsupervised clustering is a potent machine learning technique to detect the naturally distinct groups in datasets, which has been widely used in various scientific studies, such as identifying cell types from single-cell RNA sequencing data [64] and detecting enterotypes of the human gut microbiome [65]. Of note, several factors, such as clustering methodology and distance metrics, influence cluster detection [12], while no clustering

method can perform optimally across all datasets. In this study, we applied PAM clustering to ACC microbiome data, optimally detecting two distinct clusters. However, we observed a maximum prediction strength less than 0.8, an empirical threshold of moderate support for clustering [13]. This might have been due to the small data size, potential contaminants, or no considerable difference in ACC intratumoral microbiome. Potential universal contamination retained in the dataset might decrease the power of cluster detection, as it would make the microbiome more similar. Despite this, we still observed a prognostic difference between two microbial subgroups, indicating the association between microbial community and prognosis.

Whether intratumoral microbiome plays a role in prognostics is quite a vital question in cancer biology. Previous pan-cancer survival analysis based on the microbial signature revealed that ACC was one of the few cancer types where the intratumoral microbiota conferred an additional benefit to established staging systems for prognosis prediction [49]. In a landmark study by Qiao et al. [62], nasopharyngeal carcinoma was shown to harbor intratumoral bacteria, whose composition was associated with NPC relapse, while the ITB load was associated with prognosis. Surprisingly, the microbiota-based clustering in our study substantially differentiated the patients into subgroups. We also proposed that 7 genera-based signatures could serve as a prognostic marker, reaching near 0.8 of the AUC value in predicting prognosis. Some of the signatures have been revealed to be associated with solid tumors or other. For example, *Fusobacterium nucleatum* orchestrates the Toll-like receptor, microRNAs, and autophagy network to control cancer chemoresistance in colorectal cancer [66]. Furthermore, compared to current tools, such as tumor staging in ACC, microbial risk score holds promise to enhance the performance of prognostic prediction, suggesting potential clinical transformation value.

DNA mutations are among the effects of the intratumoral microbiota on cancer development [67]. The microbiota has been reported to be a vital cause of DNA damage in several types of cancers including gastrointestinal cancer [68,69]. DNA damage caused by the microbiota further increases host genetic mutations, which may finally cause tumorigenesis [70]. In agreement with these findings, we found that, in addition to gene mutations, some copy number variation such as *CDKN2A* and *ZNRF3* have mostly

occurred in the MS1 cohort with a worse prognosis. These genomic events belonging to cell cycle pathway, WNT pathway, and Hippo signaling pathway were significantly different between two subgroups, which were also mentioned in other studies focusing on bacterial effectors influencing host cell signaling cascades [68,71]. Assié et al. [10] strongly suggest that ZNRF3 is a new tumor suppressor gene related to the β -catenin pathway, which gene and the cytoband loss was enriched in the cohort with worse prognosis in our study. These consistent findings lend further credence to the causative role of the intratumoral microbiota in tumorigenesis. However, future studies are still warranted.

The activation of oncogenic pathways is another effect of the intratumoral microbiota. Many studies have uncovered that certain microbes could not only influence cytokines such as IL-6 and TNF- α directly or indirectly, but also activate the NF- κ B pathway or STAT3 pathway to promote tumor progression [70]. The association between specific taxa and the cell-cycle pathway has previously been observed [72], and the genes or microRNAs in the cell cycle were found to be differentially expressed in conventional mice compared to those of germ-free mice [73]. Moreover, the cell cycle is often associated with DNA damage. Our study found that the cell cycle was significantly enriched in the MS1 cohort, which is one of the most activated pathways in ACC [8]. Besides, we found that pathways affiliated to amino acid, carbohydrate, and cofactors and vitamins were of lower scoring in MS1 subgroup, implying the inactivation of the metabolic events above ((R) Figure S12), which supported our findings previously reported [74]. We also explored the microbes significantly correlated with the genes belonging to these pathways ((R) Figure S13), but we did not overstate the legitimacy of those findings. Given the limited sample size, overfitting could have substantially skewed the results.

ACC features indolent immunity and immunotherapy resistance [56], which refers to the suppressive immune status, showing either decreased amounts of immune cells or exhaustion of T cells, B cells, and NK cells with the downregulated tumor-killing effect in the tumor microenvironment. Scientists have shown that dysbiosis in bacterial communities in the tumor environment can either cause a chronic, pro-inflammatory immune response or modulate local immune surveillance by suppressing the antitumoral immune response [70,75,76]. Our study showed a lower proportion of immune infiltration, indicating the TME

suppression status. This corresponds to the fact that MS1, enriched with C1A (characterized as a highly steroidogenic phenotype with mainly immune suppressor cortisol) [8], was shown to be associated with a worse prognosis. Mahata et al. [77] showed that tumors induce de novo steroidogenesis in T lymphocytes to evade antitumor immunity, confirming the immune suppression role of steroids. Furthermore, we discovered that excessive hormones are distinct between the two MS cohorts, suggesting the key role of steroidogenesis in the effects of the intratumoral microbiota on the tumor microenvironment.

Technically, unlike gut or body fluid microbial studies, shotgun metagenomics sequencing is not applicable for ITB detection given the extremely low biomass of intratumoral microbes [39,61]. However, several studies using the transcriptome, 16S rRNA sequencing, and FISH technique have provided convincing evidence of the existence and location of the ITB. Fu et al. [40] showed that cultured ITB from transgenic mice with spontaneous breast cancer could promote tumor metastasis via, surprisingly, mechanical reshaping by altering the cytoskeleton. This culturomics approach could, however, hardly be extrapolated to ACC for us, as transgenic ACC mice are currently lacking, and organoids of ACC have rarely been reported, without even considering the dismal chance of capturing an ITB sequence from a patient's tumor samples given the astronomical host genetic materials. Wang et al. [77] applied a metabolomics approach by evaluating the bacterial metabolite trimethylamine N-oxide (TMAO) in breast cancer and traced the ITB that secreted TMAO. Such an approach appears more feasible in ACC, with the only problem being the rarity of the disease.

The limitations of our study include the lack of external validation and a widely accepted decontamination protocol both in silico and in IHC. Firstly, the rarity of ACC renders testing of sequencing techniques such as metagenomics and 16S rRNA extremely hard in a reasonable sample size. Functional analyses based on 16S rRNA sequencing and ex vivo culture for individual ITB is currently in progress to establish causal relationships between ITB and the host, which is still at the stage of tissue collection. Considering the rarity of the disease, it is hard to accomplish substantial specimen collection in a limited time. Additionally, the lack of fresh samples makes it hard to validate RNA-Seq-based signature designation and ITB isolation. Lastly, despite decontamination

being considered, potential contaminants might still have been retained across the entire analysis. How we processed our FFPE blocks warrants optimization. Nevertheless, our findings enable a better understanding of the biology of ACC.

CONCLUSION

In summary, our study validated the presence of intratumoral microbes in adrenocortical carcinoma and characterized distinct microbiome composition that was associated with the prognosis, with **7-genera based microbial risk score** performing well in predicting prognosis. Intratumoral microbiota could crosstalk with carcinogenic pathways such as cell cycle signaling, as well as those related to tumor immunity and metabolism. Functional analyses warrant further exploration.

METHODS

Data Acquisition

Data processed by Sheng et al. (TCGA-Z) were freely downloaded from TCMbio (<https://microbiomex.sdu.edu.cn/>). The decontamination process was detailed in the original paper [1]. These microbiome data include data with raw bacterial counts at genus and species level of ACC cohort (file “ACC_otutable_bacteria_genus.csv”, “ACC_otutable_bacteria_species.csv”), and PCPG cohort at genus level (file “PCPG_otutable_bacteria_genus.csv”). The original reads count of each sample was also supplied by Sheng et al. (file “ACC.reads.stat.csv”).

The microbial profile processed by Salzberg et al. (TCGA-S) [2,3] was kindly shared by Professor Steven Salzberg, and his team performed the microbial reads extraction from the exclusively RNA-seq data of ACC just for us. The raw dataset was unpublished and are therefore retained by the authors. Only processed analytical results are presented herein to protect proprietary research interests.

The gene expression profiles of RNA sequencing (RNA-Seq) data, including raw count and those normalized to FPKM (fragments per kilobase of transcript per million fragments mapped), were downloaded from the UCSC Xena dataset [4] (<https://xenabrowser.net/datapages/>). FPKM was further converted into TPM (transcripts per million). Gene sets for single sample gene set enrichment analysis were downloaded

from the online data repository [5], and those for GSEA were acquired from the MSigDB database [6] (<https://data.broadinstitute.org/gsea-msigdb/msigdb/release/7.5.1/>).

Somatic mutation data in the form of mutation annotation format (MAF) were captured using R package “TCGAbiolinks” (v2.16.4) [7]. Gistic2 copy number data were downloaded from the UCSC Xena dataset [4] (<https://xenabrowser.net/datapages/>). Driver gene mutations or chromosomal spans with focal recurrent amplifications and deletions, together with molecular classification of different data types, were required from the online repository referenced by Zheng et al. [8].

Clinical information of TCGA-ACC patients was derived from multiple datasets and studies. We got the most of the clinical data from the cBioPortal dataset [9] (<https://www.cbiportal.org/>). The updated data of overall survival and progression-free survival were downloaded from the website (<https://gdc.cancer.gov/about-data/publications/pancanatlas>). The defined classifications based on diverse omics were derived from the supplementary data published by Assié et al. [10].

Preprocessing microbiome data

We excluded the samples with no taxa present, resulting to 1853 genera and 76 samples in TCGA-Z dataset, while 1668 genera and 77 samples in TCGA-Z dataset. To enable cross-sample comparisons of microbial abundances, raw count data were firstly normalized using Counts Per Million (CPM) to account for variations in sequencing depth.

For each sample i and microbe j , CPM was calculated as:

$$CPM = \frac{C_{ij}}{\text{Total Reads } i} \times 10^6$$

where: 1) C_{ij} is the raw count for microbe j in sample i ; 2) Total Reads i represents the sum of all reads (including host/human reads). Unless otherwise specified, our subsequent analyses are based on CPM data, or the log transformed value.

Unsupervised Clustering for Microbiome Data

Unsupervised clustering was performed on two normalized ACC microbiome data using partition around medoids (PAM) clustering in R package “cluster” [11], a more robust clustering approach than K-means clustering. This clustering algorithm relies on predefined distance metrics, which influence the detection of natural clusters in the microbiome [12].

We performed centered log ratio (CLR) transformation on our taxonomic data, as the CLR transformation improves distributional properties by converting compositionally constrained data into approximately Gaussian-distributed variables in Euclidean space, thereby fulfilling the normality assumptions underlying parametric statistical analyses and linear modeling frameworks. We assessed the optimal cluster number with the prediction strength (PS) [13] and silhouette index [14] (SI), where a score of ≥ 0.90 for PS or ≥ 0.75 for SI supports a strong clustering. PS was computed using the function *prediction.strength* in “fpc” package[13], and SI was computed using the *pam* function in “cluster” package.

Alpha Diversity and Beta Diversity of Microbial Communities

The dissimilarity of microbial communities (beta diversity) between ACC and PCPG (pheochromocytoma and paraganglioma) or between different clusters was examined by principal coordinate analysis (PCoA) analysis based on Bray–Curtis dissimilarity which was calculated based on the relative abundance of microbial communities. Permutational multivariate analysis of variance (PERMANOVA) based on Bray–Curtis dissimilarity with 999 permutations was used to compare the difference in microbial communities between groups, which was performed using *adonis2* in R package “vegan” [15]. Function *diversity* in the package “vegan” [15] was used to estimate the alpha diversity based on the relative abundance microbial data using Shannon index which represents the richness and evenness of microbial communities [16].

Identification of Microbes with Different Abundance

PERMANOVA analysis with 999 permutations, based on Bray–Curtis dissimilarity, was performed to examine the effects of clinical factors on microbial communities. All *P*-values were further adjusted for multiple comparisons with the FDR (false discovery rate) method [17]. The clinical factors with FDR-adjusted *P*-value < 0.05 were considered confounding factors. The differentially abundant microbes between two subgroups were then identified by MaAsLin2 [18] and ANCOM [19]. Only the genera with *P*-value < 0.05 were considered as significantly different between two subgroups.

Microbial Risk Score Model Construction

The prognostic risk score was developed by multivariate Cox proportional hazards

regression with bidirectional stepwise selection to eliminate redundant variables, and the risk score was calculated as:

$$\text{Risk Score} = \sum(\beta_i \times M_i)$$

where β represents the regression coefficient and M the microbial abundance. Hazard ratios (HR) and corresponding 95% confidence intervals (CIs) were calculated in the Cox models. We got the microbial risk score (MRS) based on the candidate genera as following:

MRS= (2.38 * *Anaerococcus* abundance) + (6.151 * *Leptotrichia* abundance) + (30.56 * *Alcaligenes* abundance) + (-17.05 * *Dietzia* abundance) + (-2.879 * *Fusobacterium* abundance) + (-12.91 * *Paracoccus* abundance) + (23.98 * *Mycobacterium* abundance).

Kaplan–Meier Curves

The survival distributions were estimated with Kaplan–Meier curves, using the Log-rank test to test the significance. This was performed by functions *Surv* and *survfit* in package “survival” [20] and further plotted using *ggsurvplot* in “survminer” [21]. To explore the effects of microbial signatures on overall survival, we stratified patients into two groups according to the cutoff of the median abundance of genus.

Prognostic Prediction Measurement

Receiver operating characteristic (ROC) curves were depicted using R package “pROC” (v1.18.0) [22] and “timeROC” (v0.4) [23], and the area under the curve (AUC) was calculated to assess predictive ability. The Akaike Information Criterion (AIC) [24] is a rigorously derived measure for model selection that balances goodness-of-fit against model complexity. It quantifies the relative information loss when using a given model to approximate the true data-generating process. Smaller AIC implies better fitness of a model. Decision Curve Analysis (DCA) is a statistical method that evaluates the net benefit of a predictive model or clinical decision rule by quantifying its clinical utility across a range of risk thresholds, and this method was realized by *dca* function in R package “ggDCA” [25]. At a specific threshold probability, the model curve with the highest net benefit indicates that this model provides the greatest clinical utility for decision-making at that threshold.

Somatic Variant Analysis

Somatic variants were detected and analyzed by R package “maftools” (v2.4.12) [26]. Candidate genes were limited to driver events. To compare the frequency of variations between different groups, the *mafCompare* function was adopted. The waterfall plots showing the enriched pathways were visualized using the *oncoPrint* function in R package “ComplexHeatmap” (v2.13.1) [27].

Tumor Immune and Metabolism Estimation

The *gsva* function was used to evaluate the relative proportion of 28 immune cells in tumor using R package “GSVA” (v1.36.3) [28]. To further characterize the immune infiltrations in ACC, we also used the *deconvolve_tme* function in “IOBR” R package [29] to estimate the immune cell proportions with several methodologies containing EPIC [30], quanTlseq [31], MCPcounter [32], and IPS [5], respectively. The results were scaled within each sample for subsequent heatmap visualization. For metabolic profiling estimation, the metabolic genes of pathways were limited to KEGG subcategory in C2 category derived from msigdb dataset, and the algorithm of function *gsva* was similarly used.

Differentially Expressed Gene Analysis and Gene Set Enrichment Analysis

Differentially expressed genes were then detected using R package “limma” (v3.50.0) [33], with $P < 0.05$ as significant. Gene set enrichment analysis was performed using R package “GSEABase” (v1.50.1) [34]. KEGG pathways for *Homo sapiens* were used to ensure biological relevance, and pathways overly broad (>300 genes) or overly specific (<25 genes) were excluded to improve interpretability. False discovery rate (FDR) correction (Benjamini-Hochberg) controlled for multiple testing.

Microbe-Host Gene Interaction

To characterize the interplay between intratumoral microbiota and host gene expression, we performed systematic correlation analysis using Spearman's rank correlation (ρ), a non-parametric method [35]. This approach identifies monotonic relationships between microbial abundances (normalized CPM values) and host gene expression levels (log2-transformed TPM). The correlation with $| \rho | > 0.3$ and $P < 0.05$ were selected for visualization as network plot.

16S rRNA Staining (Direct-Labeling RNA In Situ Hybridization)

To examine the presence of intratumoral bacteria in ACC, we performed 16S rRNA staining on an in-house ACC tissue microarray (TMA) chip containing 37 formalin-fixed samples. The tissues were resected adrenal tissues from patients with ACC receiving an adrenalectomy in Huashan Hospital affiliated with Fudan University. Then, they were formalin-fixed and embedded in paraffin (wax) to create an FFPE block or paraffin block, which can be cut using a microtome to generate thin sections of tissue contained in paraffin to be stained. For downstream staining, the tissue sections were processed at 180 °C for 4–6 h. Thorough sterilization of hood, blades, and relevant instruments was carried out. We adopted a direct labeling protocol because a strong background signal was observed using digoxin-labeled probes. Briefly, paraffinized sections were dewaxed and dehydrated. Protease K was applied at room temperature. A working solution was then applied, and sections were incubated at 42 °C for 2 h. After thorough rinsing with 0.2× SSC (saline–sodium citrate) buffer, 100 μM of EUB338-cy5 probes (sequence: 5'-GCTGCCTCCGTAGGAGT-3') diluted in 1 μM of working solution were mounted and incubated at 42 °C for 12–18 h. The procedure culminated with DAPI (1:500) staining. Scrambled probes were used as the negative control, and paraffin on the same tissue block was used as a contamination control.

Immunohistochemistry (IHC) of LPS

The same TMA block was used for IHC staining against bacterial lipopolysaccharide (LPS). Briefly, the block was sliced at 5 μm and mounted, followed by deparaffinization and hydration. After antigen restoration, the section was blocked with 3% hydrogen peroxide. Goat serum was applied, and the primary antibody against *Escherichia coli* LPS (Abcam, ab35654) was applied at a dilution of 1:200 overnight, followed by a mouse anti-goat antibody (Abcam, ab205719). Diaminobenzidine (DAB) was applied, and slides were counterstained with hematoxylin. The study was approved by Huashan Institutional Review Board, HIRB.

Statistical Analysis

All analyses and visualizations were performed via R software (v4.0.2) unless otherwise

specified. We used Student's t-test for parametric statistical testing, and Wilcoxon rank test and Chi-squared test or Fisher's exact test for nonparametric statistical testing between two groups. We used NS ($P > 0.05$), $*0.05 < P < 0.01$, $**0.01 < P < 0.001$, and $*** P < 0.001$ to indicate the significance levels of P -values in this paper.

References

1. Sheng, Dashuang, Chuandi Jin, Kaile Yue, Min Yue, Yijia Liang, Xinxin Xue, Pingfu Li, et al. 2024. "Pan-Cancer Atlas of Tumor-Resident Microbiome, Immunity and Prognosis." *Cancer Letters* 598: 217077. <https://doi.org/10.1016/j.canlet.2024.217077>
2. Ge, Yuchen, Jennifer Lu, Daniela Puiu, Mahler Revsine, and Steven L. Salzberg. 2024. "Comprehensive Analysis of Microbial Content in Whole-Genome Sequencing Samples from The Cancer Genome Atlas Project." 2024.05.24.595788.
3. Gihawi, Abraham, Yuchen Ge, Jennifer Lu, Daniela Puiu, Amanda Xu, Colin S. Cooper, Daniel S. Brewer, et al. 2023. "Major Data Analysis Errors Invalidate Cancer Microbiome Findings." edited by I. B. Zhulin. *mBio* 14(5): e01607-23. <https://doi.org/10.1128/mbio.01607-23>
4. Goldman, Mary J., Brian Craft, Mim Hastie, Kristupas Repecka, Fran McDade, Akhil Kamath, Ayan Banerjee, et al. 2020. "Visualizing and Interpreting Cancer Genomics Data via the Xena Platform." *Nature Biotechnology* 38(6): 675–78. <https://doi.org/10.1038/s41587-020-0546-8>
5. Charoentong, Pornpimol, Francesca Finotello, Mihaela Angelova, Clemens Mayer, Mirjana Efremova, Dietmar Rieder, Hubert Hackl, et al. 2017. "Pan-Cancer Immunogenomic Analyses Reveal Genotype-Immunophenotype Relationships and Predictors of Response to Checkpoint Blockade." *Cell Reports* 18(1): 248–62. <https://doi.org/10.1016/j.celrep.2016.12.019>
6. Subramanian, Aravind, Pablo Tamayo, Vamsi K. Mootha, Sayan Mukherjee, Benjamin L. Ebert, Michael A. Gillette, Amanda Paulovich, et al. 2005. "Gene Set Enrichment Analysis: A Knowledge-Based Approach for Interpreting Genome-Wide Expression Profiles." *Proceedings of The National Academy of Sciences of The United States of America* 102(43): 15545–50. <https://doi.org/10.1073/pnas.0506580102>
7. Colaprico, Antonio, Tiago C. Silva, Catharina Olsen, Luciano Garofano, Claudia Cava, Davide Garolini, Thais S. Sabedot, et al. 2016. "TCGAbiolinks: An R/Bioconductor Package for Integrative Analysis of TCGA Data." *Nucleic Acids Research* 44(8): e71. <https://doi.org/10.1093/nar/gkv1507>
8. Zheng, Siyuan, Andrew D. Cherniack, Ninad Dewal, Richard A. Moffitt, Ludmila

- Danilova, Bradley A. Murray, Antonio M. Lerario, et al. 2016. "Comprehensive Pan-Genomic Characterization of Adrenocortical Carcinoma." *Cancer Cell* 29(5): 723–36. <https://doi.org/10.1016/j.ccr.2016.04.002>
9. Cerami, Ethan, Jianjiong Gao, Ugur Dogrusoz, Benjamin E. Gross, Selcuk Onur Sumer, Bulent Arman Aksoy, Anders Jacobsen, et al. 2012. "The cBio Cancer Genomics Portal: An Open Platform for Exploring Multidimensional Cancer Genomics Data." *Cancer Discovery* 2(5): 401–4. <https://doi.org/10.1158/2159-8290.CD-12-0095>
 10. Assié, Guillaume, Eric Letouzé, Martin Fassnacht, Anne Jouinot, Windy Luscap, Olivia Barreau, Hanin Omeiri, et al. 2014. "Integrated Genomic Characterization of Adrenocortical Carcinoma." *Nature Genetics* 46(6): 607–12. <https://doi.org/10.1038/ng.2953>
 11. Kaufman, Leonard, and Peter J. Rousseeuw. 1990. *Partitioning around Medoids (Program Pam)*.
 12. Koren, Omry, Dan Knights, Antonio Gonzalez, Levi Waldron, Nicola Segata, Rob Knight, Curtis Huttenhower, et al. 2013. "A Guide to Enterotypes across the Human Body: Meta-Analysis of Microbial Community Structures in Human Microbiome Datasets." *Plos Computational Biology* 9(1): e1002863. <https://doi.org/10.1371/journal.pcbi.1002863>
 13. Tibshirani, Robert, and Guenther Walther. 2005. "Cluster Validation by Prediction Strength." *Journal of Computational and Graphical Statistics* 14(3): 511–28. <https://doi.org/10.1198/106186005X59243>
 14. Rousseeuw, Peter J. 1987. "Silhouettes: A Graphical Aid to the Interpretation and Validation of Cluster Analysis." *Journal of Computational and Applied Mathematics* 20: 53–65. [https://doi.org/10.1016/0377-0427\(87\)90125-7](https://doi.org/10.1016/0377-0427(87)90125-7)
 15. Oksanen, Jari, Gavin L. Simpson, F. Guillaume Blanchet, Roeland Kindt, Pierre Legendre, Peter R. Minchin, R. B. O'Hara, et al. 2022. "Vegan: Community Ecology Package." *R Package Version 2.6-4*.
 16. McMurdie, Paul J., and Susan Holmes. 2013. "Phyloseq: An R Package for Reproducible Interactive Analysis and Graphics of Microbiome Census Data." *PLoS One* 8(4): e61217. <https://doi.org/10.1371/journal.pone.0061217>
 17. Benjamini, Yoav, Dan Draai, Greg Elmer, Neri Kafkafi, and Ilan Golani. 2001. "Controlling the False Discovery Rate in Behavior Genetics Research." *Behavioural Brain Research* 125(1): 279–84. [https://doi.org/10.1016/S0166-4328\(01\)00297-2](https://doi.org/10.1016/S0166-4328(01)00297-2)
 18. Mallick, Himel, Ali Rahnavard, Lauren J. McIver, Siyuan Ma, Yancong Zhang, Long H. Nguyen, Timothy L. Tickle, et al. 2021. "Multivariable Association Discovery in Population-Scale Meta-Omics Studies." *Plos Computational Biology* 17(11):

e1009442. <https://doi.org/10.1371/journal.pcbi.1009442>

19. Lin, Huang, and Shyamal Das Peddada. 2020. “Analysis of Compositions of Microbiomes with Bias Correction.” *Nature Communications* 11(1): 3514. <https://doi.org/10.1038/s41467-020-17041-7>
20. Therneau, Terry M., and Patricia M. Grambsch. 2000. *Modeling Survival Data: Extending the Cox Model*. 1st ed. New York, NY: Springer
21. Kassambara, Alboukadel, Marcin Kosinski, Przemyslaw Biecek, and Scheipl Fabian. 2021. “Survminer: Drawing Survival Curves Using ‘Ggplot2.’” *R Package Version 0.4.9*.
22. Robin, Xavier, Natacha Turck, Alexandre Hainard, Natalia Tiberti, Frederique Lisacek, Jean-Charles Sanchez, and Markus Muller. 2011. “pROC: An Open-Source Package for R and S+ to Analyze and Compare ROC Curves.” *BMC Bioinformatics* 12: 77. <https://doi.org/10.1186/1471-2105-12-77>
23. Blanche, Paul, Jean-Francois Dartigues, and Helene Jacqmin-Gadda. 2013. “Estimating and Comparing Time-Dependent Areas under Receiver Operating Characteristic Curves for Censored Event Times with Competing Risks.” *Statistics in Medicine* 32(30): 5381–97. <https://doi.org/10.1002/sim.5958>
24. Cavanaugh, Joseph E., and Andrew A. Neath. 2019. “The Akaike Information Criterion: Background, Derivation, Properties, Application, Interpretation, and Refinements.” *WIREs Computational Statistics* 11(3): e1460. <https://doi.org/10.1002/wics.1460>
25. Zhang, Jing, and Zhi Jin. 2025. “ggDCA: Calculate and Plot Decision Curve.” *R Package Version 1.2*. <https://github.com/yikeshu0611/ggDCA>
26. Mayakonda, Anand, De-Chen Lin, Yassen Assenov, Christoph Plass, and H. Phillip Koeffler. 2018. “MafTools: Efficient and Comprehensive Analysis of Somatic Variants in Cancer.” *Genome Research* 28(11): 1747–56. <https://doi.org/10.1101/gr.239244.118>
27. Gu, Zuguang, Roland Eils, and Matthias Schlesner. 2016. “Complex Heatmaps Reveal Patterns and Correlations in Multidimensional Genomic Data.” *Bioinformatics* 32(18): 2847–49. <https://doi.org/10.1093/bioinformatics/btw313>
28. Hanzelmann, Sonja, Robert Castelo, and Justin Guinney. 2013. “GSVA: Gene Set Variation Analysis for Microarray and RNA-Seq Data.” *BMC Bioinformatics* 14: 7. <https://doi.org/10.1186/1471-2105-14-7>
29. Zeng, Dongqiang, Yiran Fang, Wenjun Qiu, Peng Luo, Shixiang Wang, Rongfang Shen, Wenchao Gu, et al. 2024. “Enhancing Immuno-Oncology Investigations through Multidimensional Decoding of Tumor Microenvironment with IOBR 2.0.” *Cell*

30. Racle, Julien, Kaat De Jonge, Petra Baumgaertner, Daniel E. Speiser, and David Gfeller. 2017. "Simultaneous Enumeration of Cancer and Immune Cell Types from Bulk Tumor Gene Expression Data." *eLife* 6: e26476. <https://doi.org/10.7554/eLife.26476>
31. Finotello, Francesca, Clemens Mayer, Christina Plattner, Gerhard Laschober, Dietmar Rieder, Hubert Hackl, Anne Krogsdam, et al. 2019. "Molecular and Pharmacological Modulators of the Tumor Immune Contexture Revealed by Deconvolution of RNA-Seq Data." *Genome Medicine* 11(1): 34. <https://doi.org/10.1186/s13073-019-0638-6>
32. Becht, Etienne, Nicolas A. Giraldo, Laetitia Lacroix, Bénédicte Buttard, Nabila Elarouci, Florent Petitprez, Janick Selves, et al. 2016. "Estimating the Population Abundance of Tissue-Infiltrating Immune and Stromal Cell Populations Using Gene Expression." *Genome Biology* 17(1): 218. <https://doi.org/10.1186/s13059-016-1070-5>
33. Ritchie, Matthew E., Belinda Phipson, Di Wu, Yifang Hu, Charity W. Law, Wei Shi, and Gordon K. Smyth. 2015. "Limma Powers Differential Expression Analyses for RNA-Sequencing and Microarray Studies." *Nucleic Acids Research* 43(7): e47. <https://doi.org/10.1093/nar/gkv007>
34. Morgan, Martin, Seth Falcon, and Robert Gentleman. 2020. "GSEABase: Gene Set Enrichment Data Structures and Methods." *R Package Version 1.50.1*.
35. Spearman, C. 1987. "The Proof and Measurement of Association between Two Things. By C. Spearman, 1904." *The American Journal of Psychology* 100(3–4): 441–71.
36. Jin, Yi, Zhanwang Wang, Dong He, Yuxing Zhu, Xueying Hu, Lian Gong, Mengqing Xiao, et al. 2021. "Analysis of m6A-Related Signatures in the Tumor Immune Microenvironment and Identification of Clinical Prognostic Regulators in Adrenocortical Carcinoma." *Frontiers in Immunology* 12: 637933. <https://doi.org/10.3389/fimmu.2021.637933>
37. Fassnacht, Martin, Massimo Terzolo, Bruno Allolio, Eric Baudin, Harm Haak, Alfredo Berruti, Staffan Welin, et al. 2012. "Combination Chemotherapy in Advanced Adrenocortical Carcinoma." *New England Journal of Medicine* 366(23): 2189–97. <https://doi.org/10.1056/NEJMoa1200966>
38. Battaglia, Thomas W., Iris L. Mimpel, Joleen J. H. Traets, Arne Van Hoeck, Laurien J. Zeverijn, Birgit S. Geurts, Gijs F. De Wit, et al. 2024. "A Pan-Cancer Analysis of the Microbiome in Metastatic Cancer." *Cell* 187(9): 2324-2335.e19. <https://doi.org/10.1016/j.cell.2024.03.021>

39. Nejman, Deborah, Ilana Livyatan, Harold Fuks, Nancy Gavert, Yaara Zwang, Leore T. Geller, Aviva Rotter-Maskowitz, et al. 2020. "The Human Tumor Microbiome Is Composed of Tumor Type-Specific Intracellular Bacteria." *Science* 368(6494): 973–80. <https://doi.org/10.1126/science.aay9189>
40. Fu, Aikun, Bingqing Yao, Tingting Dong, Yongyi Chen, Jia Yao, Yu Liu, Hang Li, et al. 2022. "Tumor-Resident Intracellular Microbiota Promotes Metastatic Colonization in Breast Cancer." *Cell* 185(8): 1356-1372.e26. <https://doi.org/10.1016/j.cell.2022.02.027>
41. Marshall, BarryJ, and J. Robin Warren. 1984. "Unidentified Curved Bacilli in the Stomach of Patients with Gastritis and Peptic Ulceration." *Lancet* 1(8390): 1311–15. [https://doi.org/10.1016/s0140-6736\(84\)91816-6](https://doi.org/10.1016/s0140-6736(84)91816-6)
42. Brechot, Christian. 2004. "Pathogenesis of Hepatitis B Virus-Related Hepatocellular Carcinoma: Old and New Paradigms." *Gastroenterology* 127(5 Suppl 1): S56-61. <https://doi.org/10.1053/j.gastro.2004.09.016>
43. Zhou, Cheng-Bei, Yi-Lu Zhou, and Jing-Yuan Fang. 2021. "Gut Microbiota in Cancer Immune Response and Immunotherapy." *Trends in Cancer* 7(7): 647–60. <https://doi.org/10.1016/j.trecan.2021.01.010>
44. Spencer, Christine N., Jennifer L. McQuade, Vancheswaran Gopalakrishnan, John A. McCulloch, Marie Vetizou, Alexandria P. Cogdill, Md A. Wadud Khan, et al. 2021. "Dietary Fiber and Probiotics Influence the Gut Microbiome and Melanoma Immunotherapy Response." *Science* 374(6575): 1632–40. <https://doi.org/10.1126/science.aaq7015>
45. Bindels, L. B., P. Porporato, E. M. Dewulf, J. Verrax, A. M. Neyrinck, J. C. Martin, K. P. Scott, et al. 2012. "Gut Microbiota-Derived Propionate Reduces Cancer Cell Proliferation in the Liver." *British Journal of Cancer* 107(8): 1337–44. <https://doi.org/10.1038/bjc.2012.409>
46. Belcheva, Antoaneta, Thergiory Irrazabal, Susan J. Robertson, Catherine Streutker, Heather Maughan, Stephen Rubino, Eduardo H. Moriyama, et al. 2014. "Gut Microbial Metabolism Drives Transformation of MSH2-Deficient Colon Epithelial Cells." *Cell* 158(2): 288–99. <https://doi.org/10.1016/j.cell.2014.04.051>
47. Ge, Yanshan, Xinhui Wang, Yali Guo, Junting Yan, Aliya Abuduwaili, Kasimujiang Aximujiang, Jie Yan, et al. 2021. "Gut Microbiota Influence Tumor Development and Alter Interactions with the Human Immune System." *Journal of Experimental & Clinical Cancer Research* 40(1): 42. <https://doi.org/10.1186/s13046-021-01845-6>
48. Kamada, Nobuhiko, Sang-Uk Seo, Grace Y. Chen, and Gabriel Nunez. 2013. "Role of the Gut Microbiota in Immunity and Inflammatory Disease." *Nature Reviews Immunology* 13(5): 321–35. <https://doi.org/10.1038/nri3430>

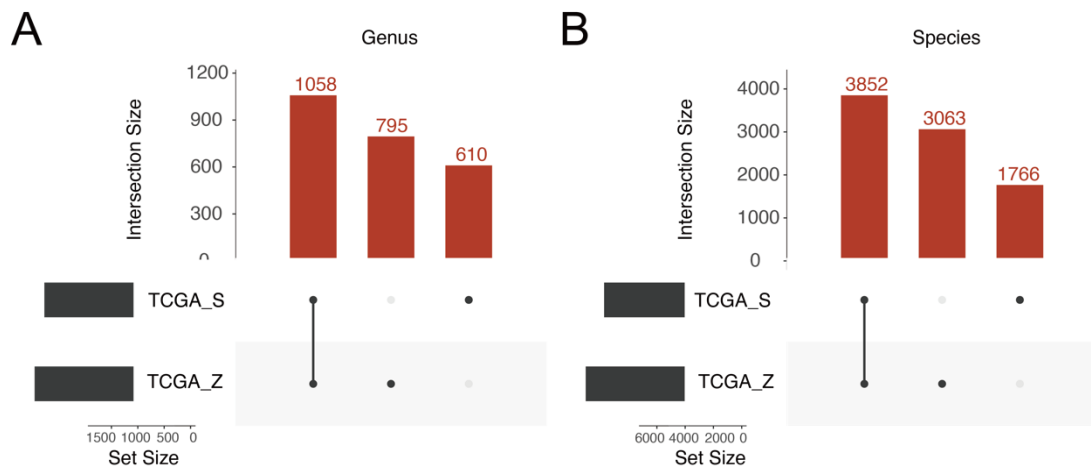
49. Hermida, Leandro C., E. Michael Gertz, and Eytan Ruppin. 2022. "Predicting Cancer Prognosis and Drug Response from the Tumor Microbiome." *Nature Communications* 13(1): 2896. <https://doi.org/10.1038/s41467-022-30512-3>
50. Goel, Manish Kumar, Pardeep Khanna, and Jugal Kishore. 2010. "Understanding Survival Analysis: Kaplan-Meier Estimate." *International Journal of Ayurveda Research* 1(4): 274–78. <https://doi.org/10.4103/0974-7788.76794>
51. Riquelme, Erick, Yu Zhang, Liangliang Zhang, Maria Montiel, Michelle Zoltan, Wenli Dong, Pompeyo Quesada, et al. 2019. "Tumor Microbiome Diversity and Composition Influence Pancreatic Cancer Outcomes." *Cell* 178(4): 795-806.e12. <https://doi.org/10.1016/j.cell.2019.07.008>
52. Luo, Mei, Yuan Liu, Leandro C. Hermida, E. Michael Gertz, Zhao Zhang, Qiang Li, Lixia Diao, et al. 2022. "Race Is a Key Determinant of the Human Intratumor Microbiome." *Cancer Cell* 40(9): 901–2. <https://doi.org/10.1016/j.ccr.2022.08.007>
53. Fragoso, Maria Candida B. V., Madson Queiroz Almeida, Tania L. Mazzuco, Beatriz M. P. Mariani, Luciana P. Brito, Talita Cardoso Goncalves, Guilherme A. Alencar, et al. 2012. "Combined Expression of BUB1B, DLGAP5, and PINK1 as Predictors of Poor Outcome in Adrenocortical Tumors: Validation in a Brazilian Cohort of Adult and Pediatric Patients." *European Journal of Endocrinology* 166(1): 61–67. <https://doi.org/10.1530/EJE-11-0806>
54. Lin, Xiaozeng, Yan Gu, Yingying Su, Ying Dong, Pierre Major, Anil Kapoor, and Damu Tang. 2022. "Prediction of Adrenocortical Carcinoma Relapse and Prognosis with a Set of Novel Multigene Panels." *Cancers (Basel)* 14(11): 2805. <https://doi.org/10.3390/cancers14112805>
55. Valero, Cristina, Mark Lee, Douglas Hoen, Jingming Wang, Zaineb Nadeem, Neal Patel, Michael A. Postow, et al. 2021. "The Association between Tumor Mutational Burden and Prognosis Is Dependent on Treatment Context." *Nature Genetics* 53(1): 11–15. <https://doi.org/10.1038/s41588-020-00752-4>
56. Georgantzoglou, Natalia, Stefania Kokkali, Gerasimos Tsourouflis, and Stamatios Theocharis. 2021. "Tumor Microenvironment in Adrenocortical Carcinoma: Barrier to Immunotherapy Success?" *Cancers (Basel)* 13(8): 1798. <https://doi.org/10.3390/cancers13081798>
57. Jin, Chengcheng, Georgia K. Lagoudas, Chen Zhao, Susan Bullman, Arjun Bhutkar, Bo Hu, Samuel Ameh, et al. 2019. "Commensal Microbiota Promote Lung Cancer Development via $\Gamma\delta$ T Cells." *Cell* 176(5): 998–1013. <https://doi.org/10.1016/j.cell.2018.12.040>
58. Parhi, Lishay, Tamar Alon-Maimon, Asaf Sol, Deborah Nejman, Amjad Shhadeh, Tanya Fainsod-Levi, Olga Yajuk, et al. 2020. "Breast Cancer Colonization by

- Fusobacterium Nucleatum Accelerates Tumor Growth and Metastatic Progression.” *Nature Communications* 11(1): 3259. <https://doi.org/10.1038/s41467-020-16967-2>
59. Sepich-Poore, Gregory D., Laurence Zitvogel, Ravid Straussman, Jeff Hasty, Jennifer A. Wargo, and Rob Knight. 2021. “The Microbiome and Human Cancer.” *Science* 371(6536): eabc4552. <https://doi.org/10.1126/science.abc4552>
 60. de Reyniès, Aurélien, Guillaume Assié, David S. Rickman, Frédérique Tissier, Lionel Groussin, Fernande René-Corail, Bertrand Dousset, et al. 2009. “Gene Expression Profiling Reveals a New Classification of Adrenocortical Tumors and Identifies Molecular Predictors of Malignancy and Survival.” *Journal of Clinical Oncology* 27(7): 1108–15. <https://doi.org/10.1200/JCO.2008.18.5678>
 61. Bullman, Susan, Chandra S. Pedamallu, Ewa Sicinska, Thomas E. Clancy, Xiaoyang Zhang, Diana Cai, Donna Neuberg, et al. 2017. “Analysis of Fusobacterium Persistence and Antibiotic Response in Colorectal Cancer.” *Science* 358(6369): 1443–48. <https://doi.org/10.1126/science.aal5240>
 62. Qiao, Han, Xi-Rong Tan, Hui Li, Jun-Yan Li, Xiao-Zhong Chen, Ying-Qin Li, Wen-Fei Li, et al. 2022. “Association of Intratumoral Microbiota With Prognosis in Patients With Nasopharyngeal Carcinoma From 2 Hospitals in China.” *JAMA Oncology* 8(9): 1301. <https://doi.org/10.1001/jamaoncol.2022.2810>
 63. Sun, Jiwei, Qingming Tang, Shaoling Yu, Mengru Xie, Wenhao Zheng, Guangjin Chen, Ying Yin, et al. 2023. “F. Nucleatum Facilitates Oral Squamous Cell Carcinoma Progression via GLUT1-Driven Lactate Production.” *eBioMedicine* 88: 104444. <https://doi.org/10.1016/j.ebiom.2023.104444>
 64. Kiselev, Vladimir Yu, Tallulah S. Andrews, and Martin Hemberg. 2019. “Challenges in Unsupervised Clustering of Single-Cell RNA-Seq Data.” *Nature Reviews Genetics* 20(5): 273–82. <https://doi.org/10.1038/s41576-018-0088-9>
 65. Arumugam, Manimozhiyan, Jeroen Raes, Eric Pelletier, Denis Le Paslier, Takaji Yamada, Daniel R. Mende, Gabriel R. Fernandes, et al. 2011. “Enterotypes of the Human Gut Microbiome.” *Nature* 473(7346): 174–80. <https://doi.org/10.1038/nature09944>
 66. Yu, TaChung, Fangfang Guo, Yanan Yu, Tiantian Sun, Dan Ma, Jixuan Han, Yun Qian, et al. 2017. “Fusobacterium Nucleatum Promotes Chemoresistance to Colorectal Cancer by Modulating Autophagy.” *Cell* 170(3): 548-563.e16. <https://doi.org/10.1016/j.cell.2017.07.008>
 67. Yang, Li, Aitian Li, Ying Wang, and Yi Zhang. 2023. “Intratumoral Microbiota: Roles in Cancer Initiation, Development and Therapeutic Efficacy.” *Signal Transduction And Targeted Therapy* 8(1): 35. <https://doi.org/10.1038/s41392-022-01304-4>
 68. Gagnaire, Aurelie, Bertrand Nadel, Didier Raoult, Jacques Neefjes, and Jean-Pierre

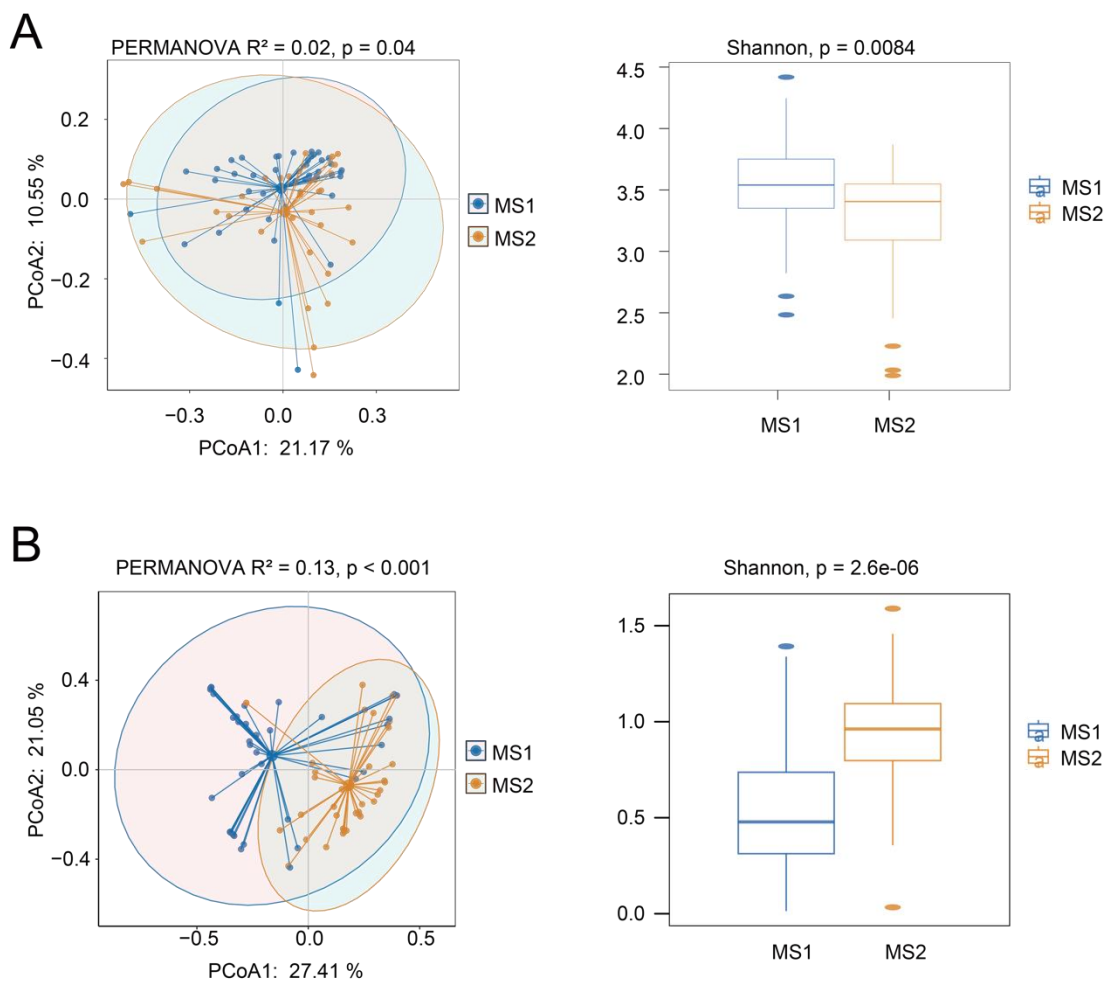
- Gorvel. 2017. "Collateral Damage: Insights into Bacterial Mechanisms That Predispose Host Cells to Cancer." *Nature Reviews Microbiology* 15(2): 109–28. <https://doi.org/10.1038/nrmicro.2016.171>
69. Janney, Alina, Fiona Powrie, and Elizabeth H. Mann. 2020. "Host-Microbiota Maladaptation in Colorectal Cancer." *Nature* 585(7826): 509–17. <https://doi.org/10.1038/s41586-020-2729-3>
70. Garrett, Wendy S. 2015. "Cancer and the Microbiota." *Science* 348(6230): 80–86. <https://doi.org/10.1126/science.aaa4972>
71. Kadosh, Eliran, Irit Snir-Alkalay, Avanthika Venkatachalam, Shahaf May, Audrey Lasry, Ela Elyada, Adar Zinger, et al. 2020. "The Gut Microbiome Switches Mutant P53 from Tumour-Suppressive to Oncogenic." *Nature* 586(7827): 133–38. <https://doi.org/10.1038/s41586-020-2541-0>
72. Nougayrede, Jean-Philippe, Stefan Homburg, Frederic Taieb, Michele Boury, Elzbieta Brzuszkiewicz, Gerhard Gottschalk, Carmen Buchrieser, et al. 2006. "Escherichia Coli Induces DNA Double-Strand Breaks in Eukaryotic Cells." *Science* 313(5788): 848–51. <https://doi.org/10.1126/science.1127059>
73. Peck, Bailey C. E., Amanda T. Mah, Wendy A. Pitman, Shengli Ding, P. Kay Lund, and Praveen Sethupathy. 2017. "Functional Transcriptomics in Diverse Intestinal Epithelial Cell Types Reveals Robust microRNA Sensitivity in Intestinal Stem Cells to Microbial Status." *The Journal of Biological Chemistry* 292(7): 2586–2600. <https://doi.org/10.1074/jbc.M116.770099>
74. Tan, Linyi, Dengwei Zhang, Yong-xin Li, Yuqing Li, Ting Guo, Yang Sun, Ning Li, et al. 2024. "Identification of Intratumor Bacteria-Associated Prognostic Risk Score in Adrenocortical Carcinoma." edited by W.-H. Chen. *Microbiology Spectrum* e03727-23. <https://doi.org/10.1128/spectrum.03727-23>
75. Gur, Chamutal, Yara Ibrahim, Batya Isaacson, Rachel Yamin, Jawad Abed, Moriya Gamliel, Jonatan Enk, et al. 2015. "Binding of the Fap2 Protein of Fusobacterium Nucleatum to Human Inhibitory Receptor TIGIT Protects Tumors from Immune Cell Attack." *Immunity* 42(2): 344–55. <https://doi.org/10.1016/j.jimmuni.2015.01.010>
76. Le Noci, Valentino, Simone Guglielmetti, Stefania Arioli, Chiara Camisaschi, Francesca Bianchi, Michele Sommariva, Chiara Storti, et al. 2018. "Modulation of Pulmonary Microbiota by Antibiotic or Probiotic Aerosol Therapy: A Strategy to Promote Immunosurveillance against Lung Metastases." *Cell Reports* 24(13): 3528–38. <https://doi.org/10.1016/j.celrep.2018.08.090>
77. Mahata, Bidesh, Jhuma Pramanik, Louise van der Weyden, Krzysztof Polanski, Gozde Kar, Angela Riedel, Xi Chen, et al. 2020. "Tumors Induce de Novo Steroid Biosynthesis in T Cells to Evade Immunity." *Nature Communications* 11(1): 3588.

<https://doi.org/10.1038/s41467-020-17339-6>

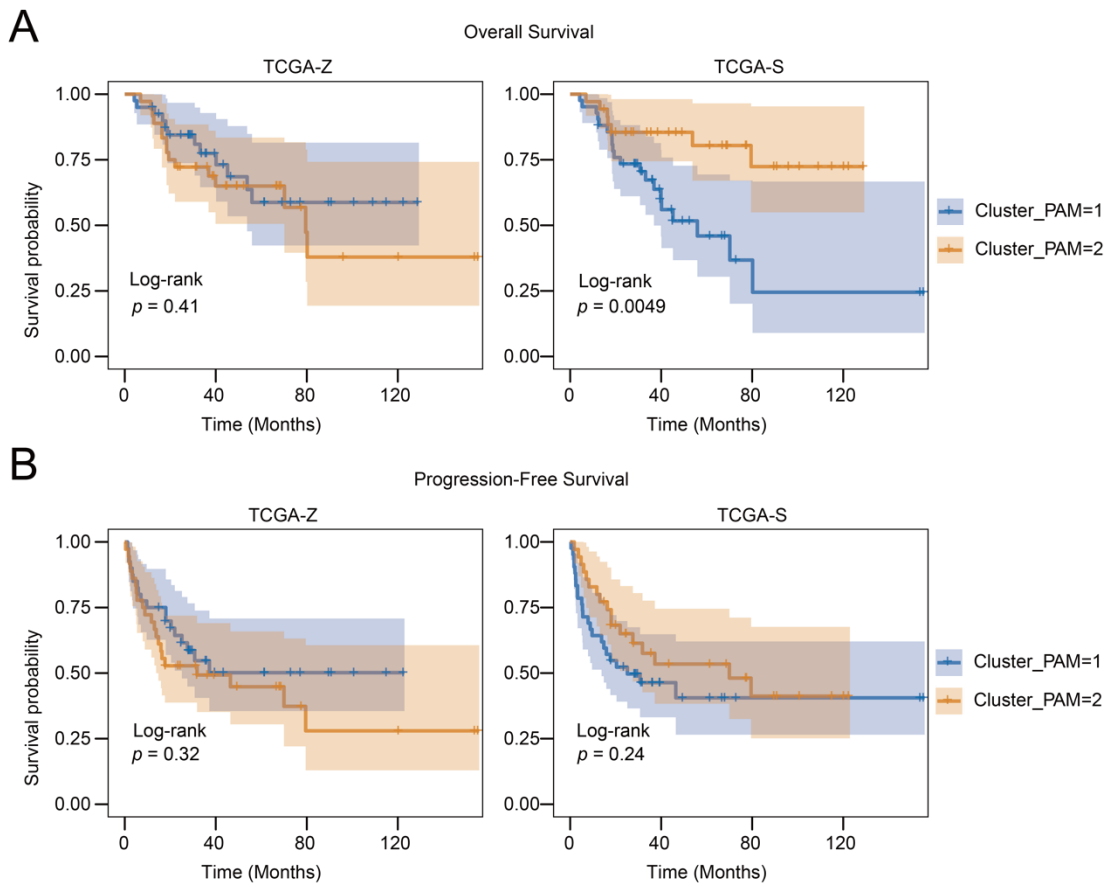
Part III Re-analyzed Supplementary Figures



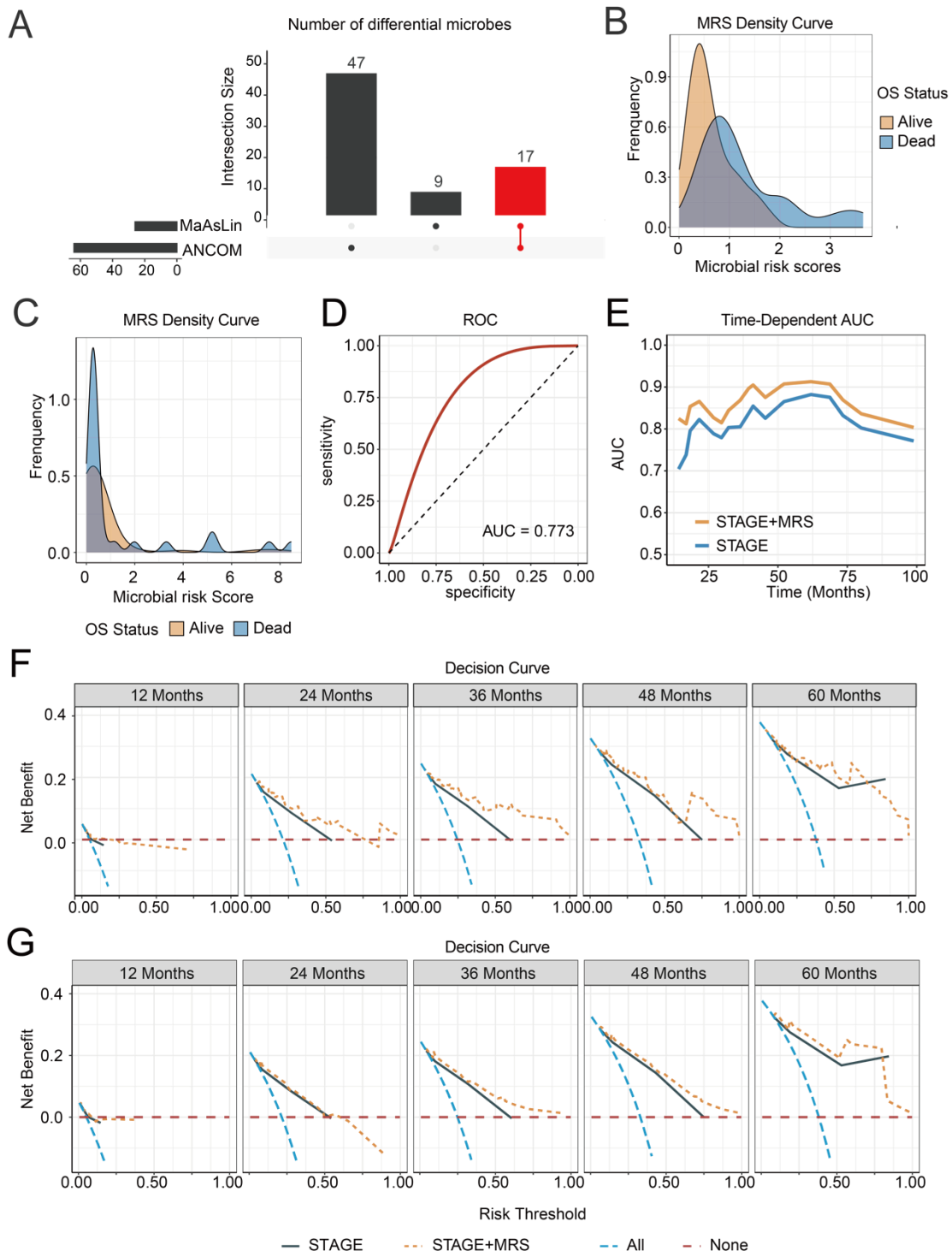
(R) Figure S1. The number of microbes detected in two datasets. The bar plot on the left refers to the number of microbes (genus (A), species (B)) included in two datasets. The bar plot on top depicts the size of each intersection. The dark dots on the bottom denote which sets are included in each intersection and are connected by lines for better visibility.



(R) Figure S2. Intratumoral microbial composition is associated with prognosis in TCGA-Z dataset. Shown are difference of beta and alpha diversity between two subgroups in (A) TCGA-S and (B) TCGA-Z clustering.

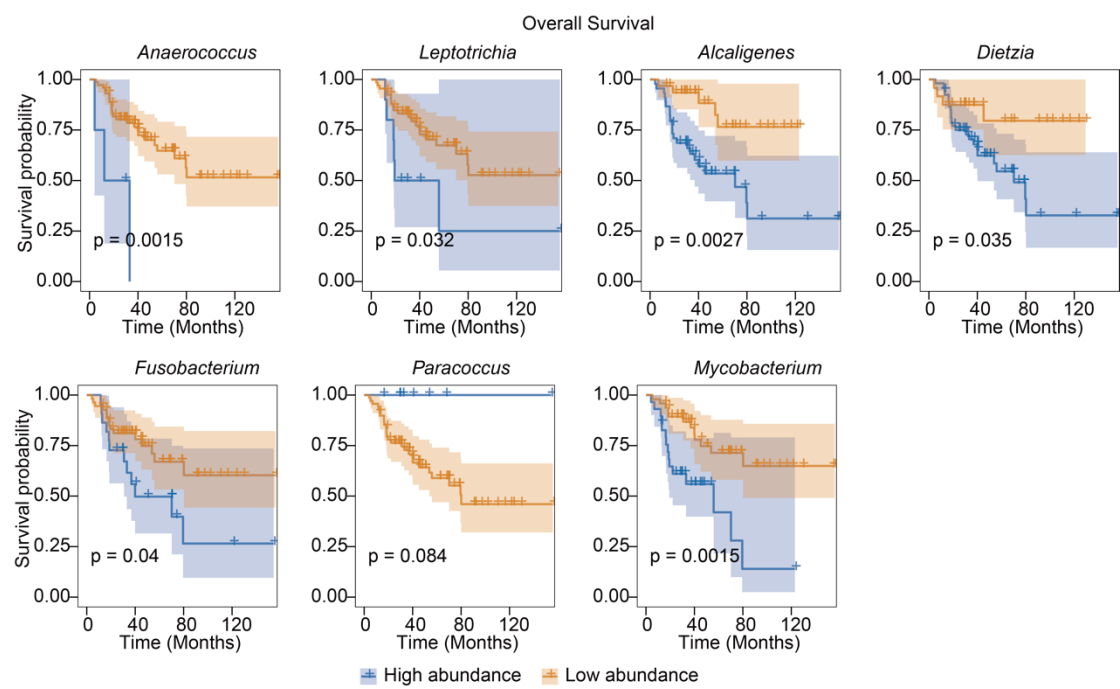


(R) Figure S3. Association between clusters and overall survival and progression-free survival. Kaplan–Meier plot of two clusters of (A) overall survival and (B) progression-free survival in two datasets. The Log-rank test gave the p value.

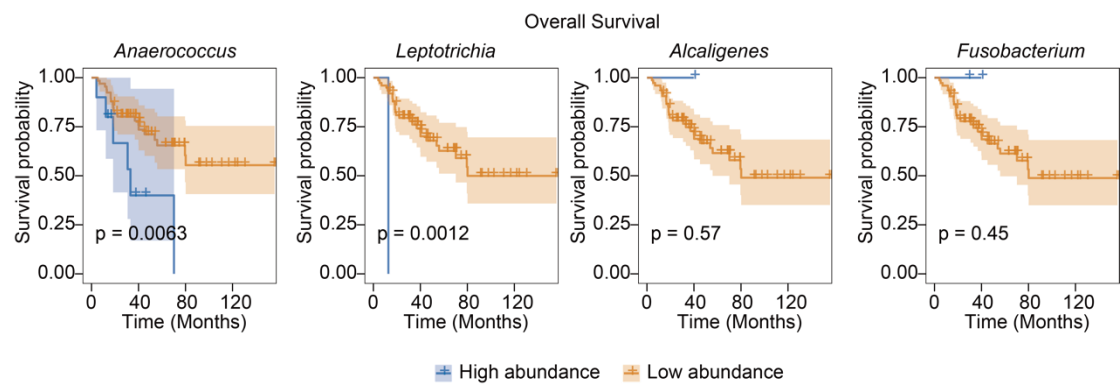


(R) Figure S4. Intratumoral microbial signatures improve prognosis prediction in TCGA-Z dataset. (A) Interaction of the genera significantly changed examined by MaAsLin2 and ANCOM between two subgroups. Density plot of the microbial risk score on OS status in (B) TCGA-S and (C) TCGA-Z dataset. (D) Receiver operation curves of 7 genera-based microbial risk score (MRS) as predictive of overall survival in TCGA-Z dataset. The area under curves suggests the predicting capability of overall survival. (E) Area under curve (AUC) for overall survival between clinical stage alone and stage plus MRS in a time-dependent manner in TCGA-Z dataset. Decision Curve Analysis (DCA) evaluating the

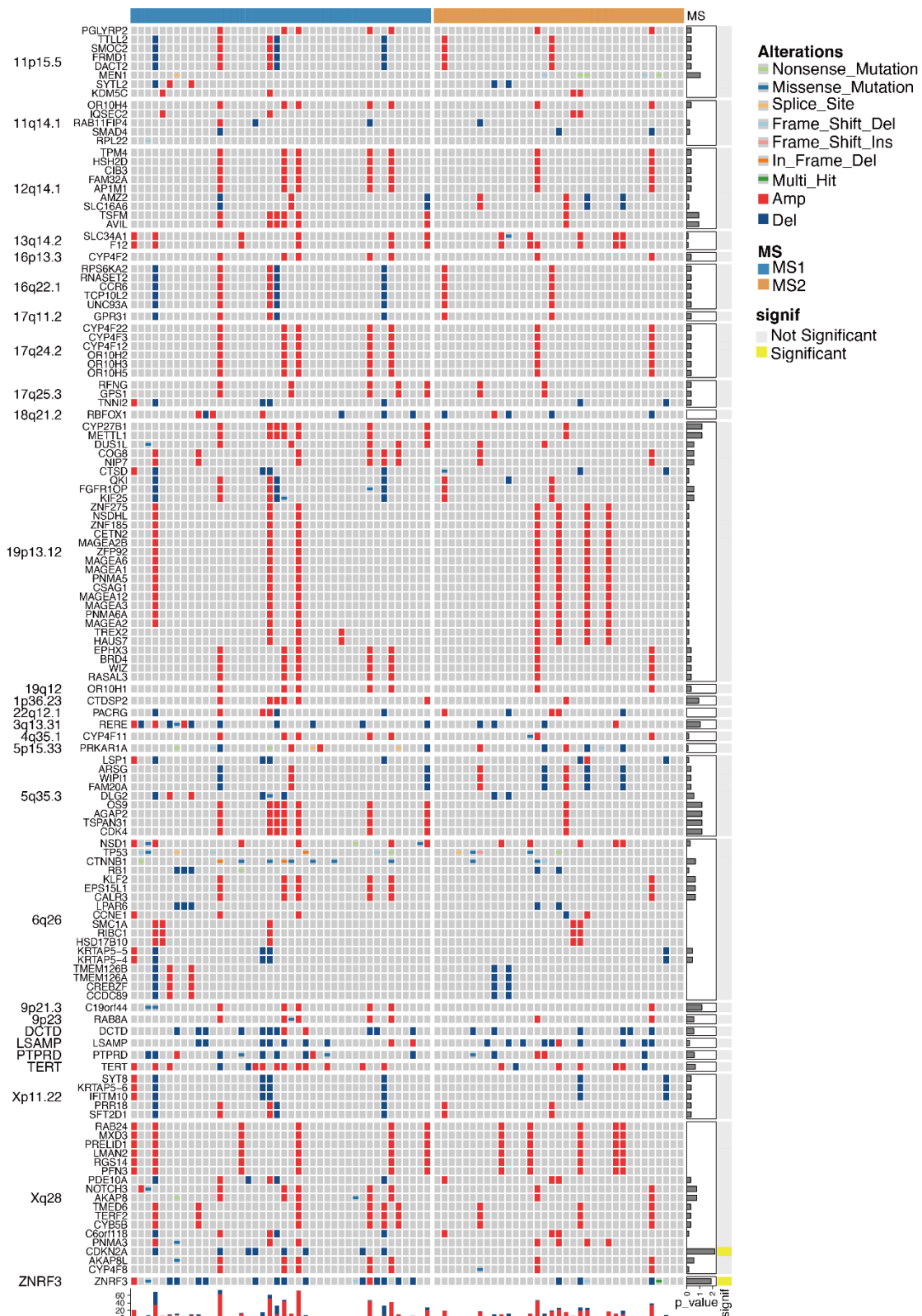
clinical benefit of the model in (F) TCGA-S and (G) TCGA-Z dataset. Shown was the net benefit curve of the models including stage and the combination of stage and MRS under different threshold at 12, 24, 36, 48, 60 months, respectively.

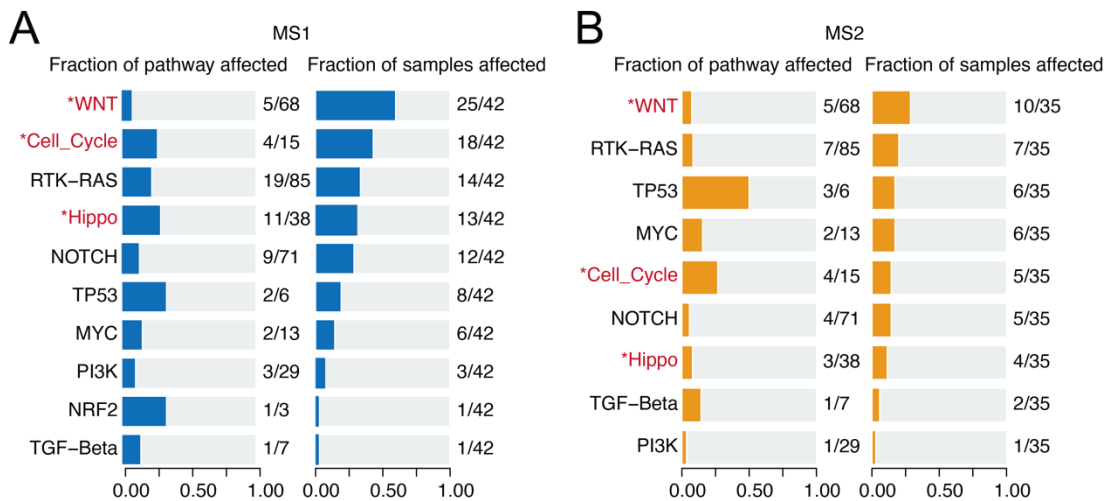


(R) Figure S5. Survival distribution based on the abundance levels of 7 microbial signatures in TCGA-S dataset. The 77 ACC patients were stratified into two groups (high abundance vs. low abundance) based on the abundance of each genus in TCGA-S data. The Log-rank test gave the p value.

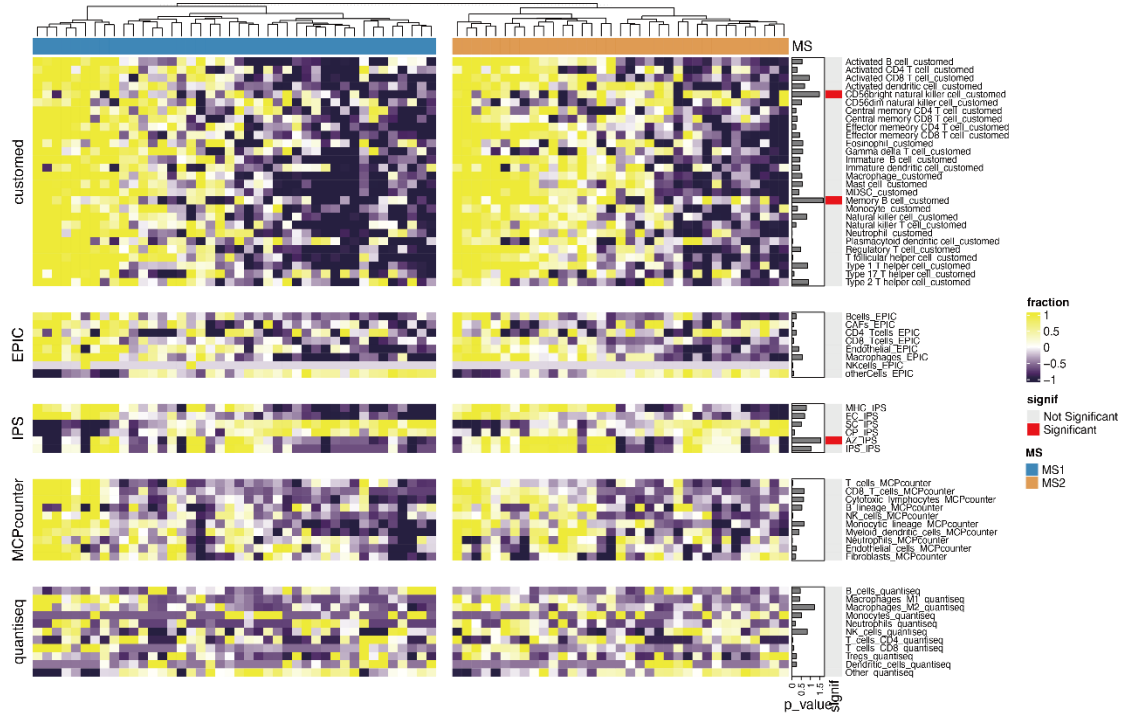


(R) Figure S6. Survival distribution based on the abundance levels of 7 microbial signatures in TCGA-Z dataset. The 77 ACC patients were stratified into two groups (high abundance vs. low abundance) based on the abundance of one of each genus in TCGA-Z data. The genus whose abundance is zero was not shown. The Log-rank test gave the p value.



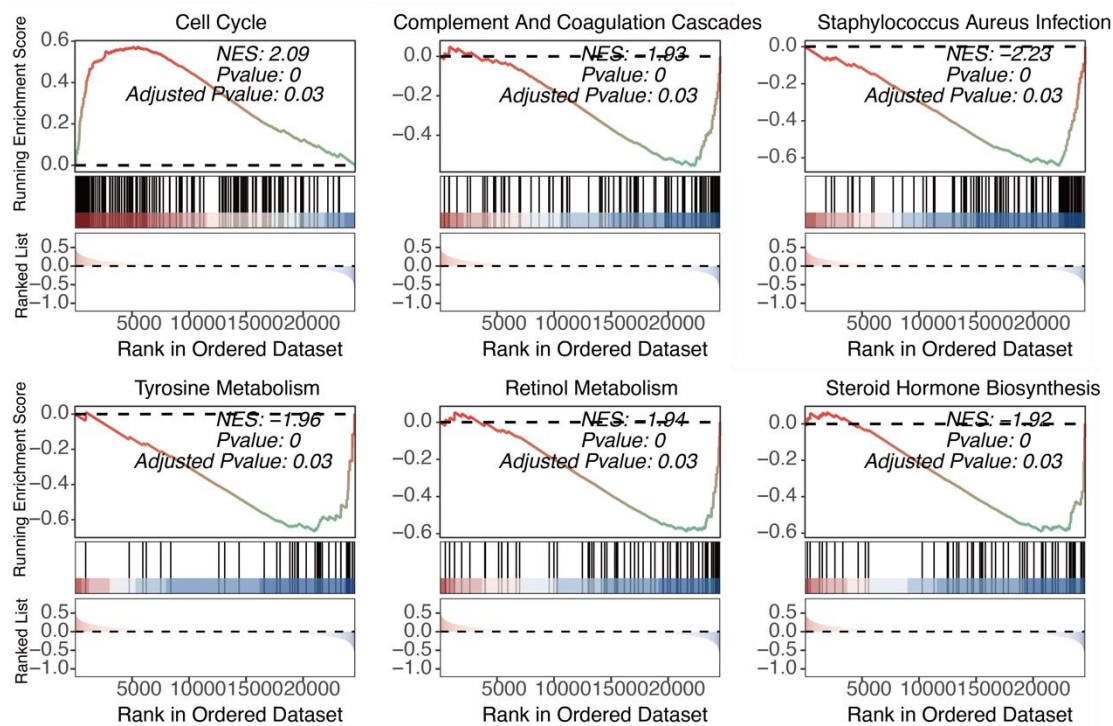


(R) Figure S8. Pathway enrichment of the genomic events within two microbial subgroups. The genomic events were observed enriched in pathways in (A) MS1 and (B) MS2 clusters. The pathway with asterisks implies significant frequency difference between two clusters.

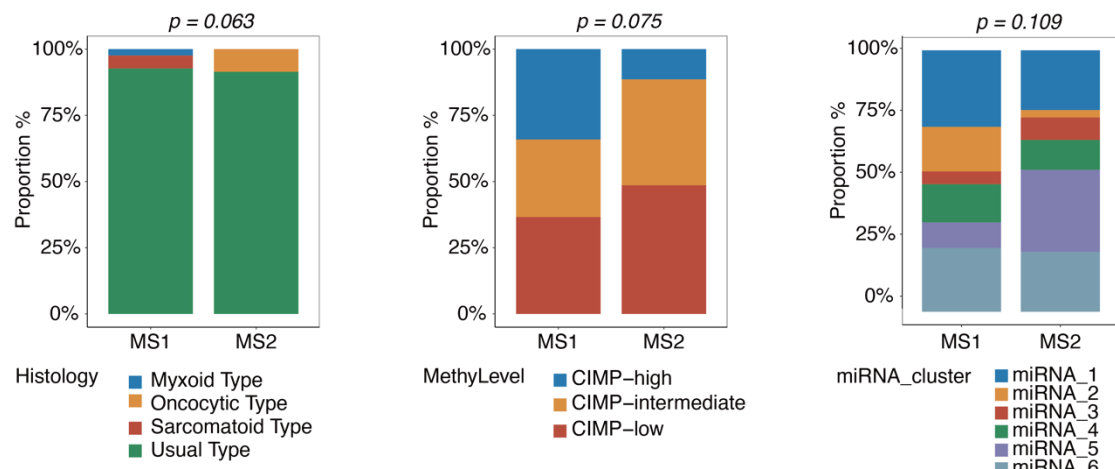


(R) Figure S9. Microbial subgroup is associated with immune cell infiltrations.

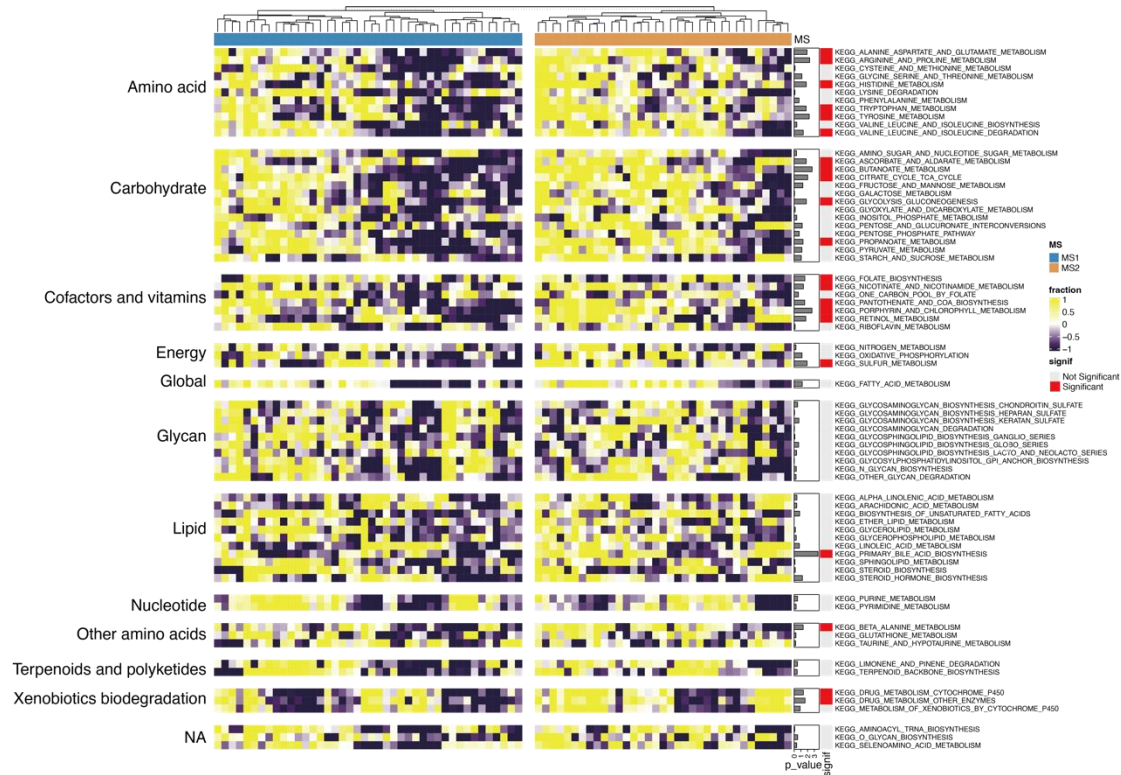
Heatmap showing the distribution of different immune cells between two clusters estimated by GSVA, EPIC, IPS, MCPcounter, and quantiseq methods.



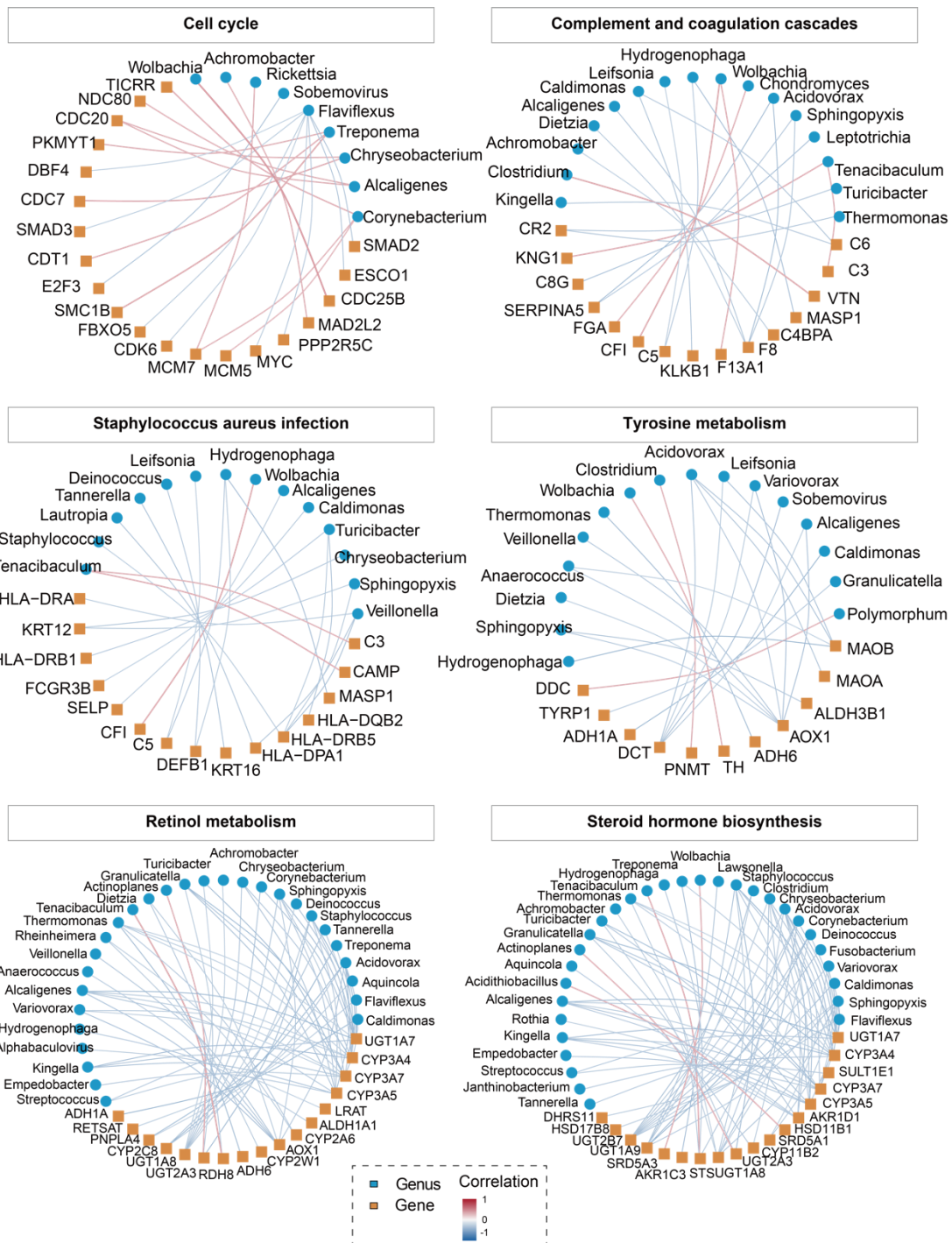
(R) Figure S10. Gene set enrichment analysis between microbial subgroups.
 Enrichment plots showing gene set enrichment results in cell cycle, complement and coagulation cascades, staphylococcus aureus infection, tyrosine metabolism, retinol metabolism, and steroid hormone biosynthesis.



(R) Figure S11. The correlation between microbial subgroup and molecular phenotypes. Stacked bar plot showing chi-squared test of (A) histology cluster, (B) methylation level cluster, (C) miRNA cluster between MS1 and MS2.



(R) Figure S12. Microbial subgroup is associated with metabolism. Heatmap showing the abundance of different metabolism-related pathways between two clusters using GSVA methods.



(R) Figure S13. Links between microbial taxa and host genes in pathways. Links between microbial taxa and host genes in the cell cycle, complement and coagulation cascades, staphylococcus aureus infection, tyrosine metabolism, retinol metabolism, and steroid hormone biosynthesis pathways. The size of circles and triangles represents the absolute value of coefficients of genes and microbes, respectively.

Part IV Re-analyzed Supplementary Tables

(R) Table S1. Chi-squared test of various clinical parameters between two subgroups.

Variable	Group	MS1	MS2	p value	
Sex	Female	28	14	0.53	
	Male	20	15		
Age	High	20	22	0.92	
	Low	18	17		
Race	Asian	0	1	0.18	
	Black or African American	1	38		
	White	0	27		
Stage	Stage I	5	9	0.71	
	Stage II	4	7		
	Stage III	18	10		
	Stage IV	19	5		
T Stage	T1	5	5	0.58	
	T2	4	3		
	T3	20	12		
	T4	22	6		
N Stage	N0	39	3	0.29	
	N1	29	6		
M Stage	M0	32	10	0.45	
	M1	30	5		
Atypical Mitotic Figures	Absent	20	15	0.22	
	Present	9	15		
Capsular Invasion	Absent	16	24	0.94	
	Present	14	18		
Clinical Status within 3 Months Surgery	Biochemical Evidence of Disease	1	9	0.58	
	No imaging evidence of disease	0	6		
	Persistent distant metastases	28	2		
	Persistent locoregional disease	26	0		
Cytoplasm =< 25%	Presence	Absent	5	30	0.76
		Present	5	19	
Diffuse Architecture	Absent	11	24	1	
	Present	8	17		
History	Adrenal	Absent	12	28	0.39
Hormone Excess		Present	14	19	
Laterality	Left	21	21	0.37	
	Right	22	13		
Mitotic Rate > 5/50 HPF	Absent	19	21	0.4	
	Present	10	19		
Necrosis	Absent	8	33	0.56	
	Present	9	23		

Nuclear Grade III or IV	Absent		6	29	0.54
	Present		7	19	
Pharmaceutical Tx	No		12	29	0.57
Adjuvant	Yes		13	21	
Pharm Tx Mitotane	No		2	23	1
Adjuvant	Yes		2	16	
Pharm Tx Mitotane	No		10	2	1
Therapeutic at Rec	Yes		6	2	
Radiation Treatment	No		30	11	0.15
Adjuvant	Yes		29	4	
Residual Tumor	R0		27	7	0.37
	R1		28	2	
	R2		4	4	
	RX		2	2	
Sinusoid Invasion	Absent		15	20	0.003
	Present		20	4	
Treatment Outcome	Complete Remission/Response		14	5	0.1
First Course	Progressive Disease		20	0	
	Stable Disease		11	1	
Tumor Status	Tumor Free		17	24	0.06
	With Tumor		23	12	
Weiss Venous Invasion	Absent		19	20	0.21
	Present		20	10	
Tumor Weight	High		18	24	0.44
	Low		19	16	

(R) Table S2. PERMANOVA test on clinical factors.

Variable	R2	F	Pr(>F)	Adj p value	Cohort
Sex	0.01	0.76	0.598	0.902	TCGA-Z
Age	0.01	0.60	0.734	0.902	
Race	0.07	2.43	0.004	0.072	
Stage	0.03	0.79	0.721	0.902	
T Stage	0.04	0.98	0.482	0.902	
N Stage	0.01	0.61	0.736	0.902	
M Stage	0.01	0.61	0.726	0.902	
Nuclear Grade III or IV	0.03	2.05	0.059	0.531	
Tumor Status	0.02	1.49	0.169	0.7965	
Atypical Mitotic Figures	0.01	0.59	0.763	0.902	
Capsular Invasion	0.01	0.61	0.72	0.902	
History Adrenal Hormone Excess	0.08	0.78	0.817	0.902	

Sex	0.01	1.01	0.393	0.851	TCGA-S
Age	0.01	0.69	0.824	0.851	
Race	0.02	0.80	0.563	0.851	
Stage	0.04	0.93	0.581	0.851	
T Stage	0.04	0.98	0.484	0.851	
N Stage	0.01	0.92	0.52	0.851	
M Stage	0.01	0.95	0.447	0.851	
Nuclear Grade III or IV	0.02	1.23	0.215	0.851	
Tumor Status	0.01	0.97	0.454	0.851	
Atypical Mitotic Figures	0.01	0.83	0.637	0.851	
Capsular Invasion	0.01	0.81	0.673	0.851	
History Adrenal Hormone Excess	0.08	0.81	0.849	0.851	

(R) Table S3. Chi-squared test of various genomic events between two subgroups.

Hugo Symbol	MS1	MS2	p value	Adj p value	Cytoband
CDKN2A	8	0	0.0067	1	9p21.3
ZNRF3	17	5	0.0128	1	22q12.1